AD_____

CONTRACT NO: DAMD17-88-C-8125

TITLE: SPECTROSCOPY OF BURN WOUNDS

PRINCIPAL INVESTIGATORS: Martin A. Afromowitz, Ph.D.
James D. Callis, Ph.D.

CONTRACTING ORGANIZATION: University of Washington
School of Medicine
Seattle, WA 98195

REPORT DATE: May 5, 1992

TYPE OF REPORT: Annual Report

PREPARED FOR: U.S. ARMY MEDICAL RESEARCH AND DEVELOPMENT COMMAND
Fort Detrick, Frederick, Maryland 21702-5012

DISTRIBUTION STATEMENT: Approved for public release;
distribution unlimited

The findings in this report are not to be construed as an official Department of the Army position unless so designated by other authorized documents.

REPORT DOCUMENTATION PAGE

Form Approved
OMB No. 0704-0188

1. AGENCY USE ONLY *(Leave blank)*	2. REPORT DATE	3. REPORT TYPE AND DATES COVERED
	5 May 1992	Annual Report (7/15/90 - 7/14/91)

4. TITLE AND SUBTITLE
SPECTROSCOPY OF BURN WOUNDS

5. FUNDING NUMBERS
Contract No.
DAMD17-88-C-8125

63002A
3M263002D840.DA.001
WUDA315068

6. AUTHOR(S)
Martin A. Afromowitz, Ph.D.
James D. Callis, Ph.D.

7. PERFORMING ORGANIZATION NAME(S) AND ADDRESS(ES)
University of Washington
School of Medicine
Seattle, WA 98195

8. PERFORMING ORGANIZATION REPORT NUMBER

9. SPONSORING/MONITORING AGENCY NAME(S) AND ADDRESS(ES)
U.S. Army Medical Research and Development Command
Fort Detrick
Frederick, Maryland 21702-5012

10. SPONSORING/MONITORING AGENCY REPORT NUMBER

11. SUPPLEMENTARY NOTES

12a. DISTRIBUTION/AVAILABILITY STATEMENT
Approved for public release; distribution unlimited

12b. DISTRIBUTION CODE

13. ABSTRACT *(Maximum 200 words)*

This research seeks to develop non-invasive burn depth evaluation methods from non-contacting visible and near-infrared spectroscopic measurements. In previous years, we demonstrated that features of the optical reflection spectra of burn wounds can be correlated with the depth of burn. An imaging system was built which determined, with accuracy equal to or better than that of a skilled burn surgeon, the probability that burn sites would heal within three weeks from date of injury. Our goal for the current project is to investigate the optical reflectance properties of burns, utilizing the techniques of multivariate analysis, in order to improve the reliability of this instrument.

14. SUBJECT TERMS
RA II; Volunteers; Diagnosis; Burn Wounds; Burn Depth; Instrument; Burn Injuries

15. NUMBER OF PAGES

16. PRICE CODE

17. SECURITY CLASSIFICATION OF REPORT	18. SECURITY CLASSIFICATION OF THIS PAGE	19. SECURITY CLASSIFICATION OF ABSTRACT	20. LIMITATION OF ABSTRACT
Unclassified	Unclassified	Unclassified	Unlimited

FOREWORD

For the protection of human subjects, the investigator(s) have adhered to policies of applicable Federal Law 45CFR56.

Citations of commercial organizations and trade names in this report do not constitute an official Department of the Army endorsement or approval of the products or services of these organizations.

ABSTRACT

This research seeks to develop non-invasive burn depth evaluation methods from non-contacting visible and near-infrared spectroscopic measurements. In previous years, we demonstrated that features of the optical reflection spectra of burn wounds can be correlated with the depth of burn. An imaging system was built which determined, with accuracy equal to or better than that of a skilled burn surgeon, the probability that burn sites would heal within three weeks from date of injury. Our goal for the current project is to investigate the optical reflectance properties of burns, utilizing the techniques of multivariate analysis, in order to improve the reliability of this instrument.

Excellent progress has been made toward achievement of the goals of this project. In the first year a commercial spectrophotometer was purchased and modified to make optical reflection measurements in both the visible and near-infrared regions (450-1800 nm). A library of reference spectra was acquired with this instrument.

During the second year, experiments were conducted to understand the major components of the reflectance spectra of human skin *in vivo*. Two dynamic processes which influence *in vivo* spectra were studied to improve our knowledge of burn physiology: temperature and ischemia. These were modeled in healthy human subjects. The spectrum of pure water, which is highly temperature dependent and dominates the spectra of biological tissues, was mathematically analyzed for the purpose of compensating for water absorbances in tissues.

Thirty four patients at Harborview Burn Center were studied, and the reflectance spectra of their burns analyzed with multivariate statistics. An unexpected absorption band correlating to burn depth was observed at 630 nm and was identified as arising from methemoglobin. Based on the foregoing results, a more reliable algorithm was developed for the imaging system. The new algorithm incorporates wavelengths which measure this methemoglobin absorption. It has been tested by simulating imaging system responses from spectrophotometer data. The new model predicts the healing potential of 110 burn sites with 88% accuracy, significantly better than simulated responses from the old imaging system (79%).

INTRODUCTION

Burn injuries affect more than two million American victims each year. Two hundred thousand of these will require hospitalization and 10,000 will die.[1] Skin grafting has significantly reduced infection, mortality, and disfigurement in patients with deep wounds. Shallow wounds, however, produce smoother skin when they are allowed to heal on their own. As a general rule, only burns which do not heal in 21 days benefit from grafting[2,3]. An accurate diagnosis may be obtained by waiting for 3 weeks before deciding to operate, but it has been shown that grafting within the first few days produces better surgical results and reduces hospital stay[*2]. This has been the driving force behind the development of methods to predict potential healing times.

For a wound to heal well (and within 21 days), it must re-epithelialize from remnants of epithelium in the lining of ducts and hair follicles. No one has yet proposed a method to predict healing by measuring the abundance of epithelium. Instead, most estimate the depth of irreparably damaged tissue with respect to the total thickness of the dermis.

Many hospitals today use a technique called clinical assessment which combines visual inspection with simple tests, such as the wound's sensitivity to touch[4]. Data collection, even for the largest and most variegated wounds, requires less than 15 minutes and does not cause excessive pain, neither from the tests themselves or from prolonged exposure of the wound. However, the accuracy of this technique is highly dependent on the experience of the assessor. Other techniques, including histopathological inspection,[5,6,7] topical application of dyes,[8] radio isotope studies,[9] ultrasound,[10] thermography,[11,12]pulse oximetry,[13] laser doppler flowmetry,[14,15] and multispectral photographic analyzers,[16,17] have proven to be slower, more painful, or less reliable and are less commonly used.

The Burn Depth Indicator

In 1980 we built the Burn Depth Indicator (BDI), a hand-held probe which illuminated a 3 cm^2 area of wound with pulsed light from three LED chips and measured the reflected light. This technique proved to be as fast as clinical assessment, less painful, and significantly more reliable.[18,19] We developed a similar instrument in 1986, which provided spatially resolved burn wound diagnosis. This device, the Imaging Burn Depth Indicator (IBDI), produces a color-coded image of a wound.[20,21,22]

Selection of the wavelengths used by the BDI (green (550 nm), red (640 nm), and near infrared (880 nm)) was based on the visible appearance of burn wounds and the discovery that near infrared light is reflected more by deep burns than shallow.*[16] Van Liew interpreted the BDI measurements in terms of blood volume, blood oxygenation, and eschar thickness. The results of his model agreed well with both the measured data and the expected physiology.*[19,23]

Spectroscopic Oximetry <u>in vivo</u>

Measurement of blood oxygenation by spectral analysis of reflected or transmitted light is a well established method. Visible (400-700 nm) and short-wave near infrared (700-1100 nm) light have been employed. Hemoglobins have $\pi \rightarrow \pi^*$, $d \rightarrow d^*$ and $f \rightarrow f^*$ electronic transitions in this region. Oxidation and ligand binding influence the spectrum substantially (Figure 1). A non-invasive oximeter, the Pulsed Oximeter,[24] now common in hospitals, uses transmission of 660 and 920 nm light through a finger tip. Its results correlate well with arterial blood O_2 saturation measured by conventional, invasive methods.[25] The success of this method has stimulated research on other non-invasive, spectrophotometric oximeters. These new instruments measure either transmitted or

reflected light and have been applied to the head,[26,27] brain,[28] heart,[*28] and skin.[*28,29] These methods are rarely calibrated to give absolute values, due to the unavailability of reference data, but they are quite useful for clinical trend monitoring and kinetic studies, where relative changes are important.

Near Infrared Spectroscopy

Near infrared light (700-2500 nm) is absorbed by other biological components besides hemoglobins. Most near infrared (NIR) absorbances are due to overtones and combination bands of vibrational transitions, primarily C-H, N-H, and O-H. This region has been used in the agricultural and food processing industries to determine, for instance, protein, oil, and moisture content.[30,31] Samples are frequently analyzed in solid or powdered form by diffuse reflectance. The resulting absorption bands, despite the high degree of light scatter in the samples, are often linear with concentration. However the spectral bands are broad and overlapping, making analysis difficult. Calibrations are therefore based on empirically observed spectral behavior rather than on first principle considerations.

Multivariate Statistics

The key that has unlocked the potential of NIR spectroscopy is multivariate statistics, mathematical methods for analyzing data sets which include multiple measurements for each sample. For spectroscopy, each filter or each monochromator setting is used to obtain different information, producing a response vector for each sample. Multivariate statistics assists the analyst to find an empirical mathematical model which will best reproduce the values of one or more constituents, given the response

vectors of a set of calibration samples. Once the model is obtained, it may be used to estimate values for prediction samples, those whose constituents are unknown.

Constituents are usually chemical concentrations, but may also be physical properties, e.g. crystallinity of nylon yarns, or abstract properties, e.g. the loaf score of flour (the volume, appearance, texture, and spring of bread made with that flour) (31). The property needs only to have some systematic relation to the spectra. Multivariate statistics can be used to analyze the spectra of burn injuries to estimate healing potential, blood oxygenation, and other properties. Further, the results of these analyses and a more precise understanding of the spectra of burned skin can be used to optimize the algorithm currently used by the IBDI.

EXPERIMENTAL

Human Subjects

Forty-three patients were studied at the Northwest Burn Center, Harborview Medical Center in Seattle, Washington, over a 13 month period. One fifth of the injuries were selected by the research nurse to give a representative sample of typical superficial, shallow partial, deep partial, and full thickness burns. The remainder were chosen because they were indeterminant or unusual. The medically fragile, including elderly, hemophiliac, and mentally ill patients, were excluded. Children were also excluded.

Patients were examined on the third day post-burn as was done in previous studies.*[18] A few of the unusual injuries were studied on the fourth day, because the patients were transferred from other hospitals and were not available on the third day.

Two to five sites were chosen by the research nurse, often with the recommendation of the attending physician. After routine cleaning and debridement

(removal of loose dead tissue), these sites were wrapped in cellophane to prevent drying and infection. Large wounds were rebandaged, except for the selected sites. The patient was then returned to his own room and positioned either in bed or in a chair. The cellophane was removed prior to spectral data acquisition.

One spectrum was acquired from each site, using an LT Quantum 1200 spectrophotometer[32] which was modified for this project. Site locations were recorded on polaroid photographs. This procedure generally took 15 to 30 minutes, including the time required to position the patient and to remove the equipment afterwards. If the patient was willing, IBDI images were also acquired, generally requiring another 10 to 20 minutes.

The injuries were followed by visual inspection for one month. The sites from which spectra had been acquired were classified according to outcome into three categories: Shallow (healed in less than 21 days), Deep (healed in more than 21 days), and Unknown. Most sites which were grafted were classified as deep. Those which were clearly shallow but were excised due to their proximity to a more severe injury were classified as shallow. If an injury was not grafted, it was inspected by the research nurse on or near the 21st day to determine if it had healed. When that was not possible, the information was obtained by phoning the patient. Sites for which there was insufficient information were classified as unknown and were excluded from analysis.

Of the sites whose outcomes were known, 34 were deep and 76 were shallow. The most common etiology was flame (52%), followed by scald (22%), chemical (8%), flash (8%), contact (6%), and grease (4%). The mean age of the patients was 33 years and the mean TBSA was 6%. There were 3 hispanics, 2 blacks, and 1 oriental. Burn locations included face, arms, hands, palms, backs, sides, legs, and feet.

Mathematical Methods

The multivariate mathematical methods needed to interpret data include preprocessing, calibration, and classification techniques. The goal is to find a useful relationship between a sample's spectrum (**r**) and the values of its constituents (**c**). Constituents are usually chemical concentrations, but may also be physical properties, abstract properties, or classifications. The property needs only to have some systematic relation to the spectra.

The notation used will be as follows: Matrices will be written in bold, upper case (**A**, **B**, **C**), row vectors in bold, lower case (**a**, **b**, **c**), and scalars in normal italic (*A*, *B*, *C*, *a*, *b*, c). Column vectors will be written as the transpose of row vectors ($\mathbf{a}^T$, $\mathbf{b}^T$, $\mathbf{c}^T$). Each spectrum will be referred to as a response row vector **r**, with length *J*, where *J* is the number of discrete wavelengths contained in each spectrum. *I* spectra grouped into a matrix will be **R**, with dimensions *I* by *J*. The elements of **R** will be written as r_{ij}. The matrix **C**, will be *I* by *K*, where *K* is the number of spectrally distinguishable constituents. The elements of **C** are c_{ik}.

Preprocessing

Preprocessing transforms the spectra such that the spectral features which correlate to the constituents are maximized and the remainder are minimized. The first step is usually linearization with respect to constituent concentration. Normally the logarithm of instrument response (*R*) is used for linearization:

$$R = I / I_0 \qquad (1)$$

where I_0 is the intensity of the light incident on the sample and *I* is the intensity of the light that returns from the sample and is measured by the instrument. The sample absorbance

(*A*) is

$$A = -\log_{10}(R) \tag{2}$$

and is proportional to analyte concentration (*c*) under certain conditions. The Beer-Lambert law is

$$A = a\,b\,c \tag{3}$$

where *b* is the path length, the distance the radiation traveled through the sample, and *a* is the molar absorptivity, a constant characteristic of the analyte. For a more complex sample, the sample absorbance (A_{ij}) is a linear sum of the absorbances of all components:

$$A_{ij} \equiv -\log_{10}(I_{ij} / I_{0,j}) \tag{4}$$

I_{ij} = intensity of radiation returned from the i^{th} sample at the j^{th} wavelength

$I_{0,j}$ = intensity of incident radiation at the j^{th} wavelength

$$A_{ij} = {}_k\Sigma\, A_{ijk} = b_i\,({}_k\Sigma\, a_{jk}\, c_{ik}) \tag{5}$$

A_{ij} = i^{th} sample absorbance at the j^{th} wavelength

A_{ijk} = absorbance of the k^{th} component in the i^{th} sample at the j^{th} wavelength

a_{jk} = absorptivity of the k^{th} chemical component at the j^{th} wavelength,

b_i = path length of light through the i^{th} sample

c_{ik} = concentration of the k^{th} analyte in the i^{th} sample

It is assumed that all of the radiation travels the same distance through the sample so that b_i is constant for all rays. For diffuse reflectance, this is not strictly true, but it is often a useful approximation.

Other common transformations include mean centering, baseline subtraction, and derivatives. The equation for mean centering is

$$(\mathbf{r}_j^T)_{\text{mean centered}} = \mathbf{r}_j^T - 1/J\ \Sigma(r_{ij}) \tag{6}$$

where $\mathbf{r}_j^T$ is the column vector of $\log(1/R)$ for the j^{th} wavelength and all samples. Baseline subtraction is

$$(\mathbf{r}_i)_{\text{baseline corrected}} = \mathbf{r}_i - r_{i,Jb} \quad (7)$$

where $\mathbf{r}_i$ is the spectrum for sample i and $r_{i,Jb}$ is the absorbance at the J_b^{th} wavelength.

An estimation of the second derivative using a finite difference function is

$$f'' \approx (f_{j+g} - 2f_j + f_{j-g}) / g^2 \quad (8)$$

where f_j is the intensity at the j^{th} wavelength and g represents the gap size of the derivative.

Calibration

Calibration is used for continuous constituent values, such as chemical concentrations or physical properties. Calibration models must be validated before they may be used for prediction. In calibration, a model is developed that relates the spectra data matrix (**R**), composed of the spectra vectors $\mathbf{r}_i$, to the constituent matrix (**C**), composed of the elements c_{ik}, for a set of samples, called the training set or the calibration set (designated by the subscript $_c$). A second set is used for validation. The model is used to predict the constituent values of the second set. Poor prediction indicates that either irrelevant data, such as instrument noise was included in the calibration model (overfitting) or that there is variance in the validation set that was not present in the training set, such as a new component. Once the model has been validated, it may be used to predict the constituents of unknown samples (designated by the subscript $_p$).

Another method of validation, leave-one-out cross validation, is useful when there are only a few spectra available. Instead of dividing the set in two, half for the calibration set and half for the prediction set, all samples except one are used for the calibration set

and the remaining sample becomes the prediction set. This is repeated *I* times, leaving out and predicting each spectra once. The result gives an estimate of the accuracy of the model that uses all *I* samples. Since the spectra acquired from different sites on the same wound may be highly correlated, this approach was modified: all spectra from a single patient were left out and predicted together.

Classical Least Squares

The calibration model generally consists of a vector of matrix of coefficients (**S**) that relates the constituent matrix to the spectral matrix. The coefficients are typically estimated by least squares or similar methods. The most straight forward methods calculate **S** assuming the Beer-Lambert relationship.

Classical least squares (CLS) is a direct calibration technique based on the Beer-Lambert law, which in matrix form is

$$\mathbf{R} = \mathbf{C}\,\mathbf{S} + \mathbf{E}_R \tag{9}$$

where **S** is the estimated pure component spectra ($s_{jk} \approx a_{jk}\, b_{ij}$) and $\mathbf{E}_R$ is the matrix of spectral errors. The **S** matrix is determined by

$$\mathbf{S} = \mathbf{R}_c\, \mathbf{C}_c^{+} \tag{10}$$

where $\mathbf{R}_c$ and $\mathbf{C}_c$ are the spectral and concentration matrices of the training set. $\mathbf{C}^{+}$ is the Moor-Penrose pseudoinverse:[33]

$$\mathbf{C}^{+} = (\mathbf{C}^{T}\,\mathbf{C})^{-1}\,\mathbf{C}^{T} \tag{11}$$

By solving these equations, $\mathbf{E}_R$ is minimized in a least squares sense. The estimated concentrations $(\hat{\mathbf{c}}_p^{\,T})_i$ of all *k* components in the i^{th} unknown sample with spectrum $(\mathbf{r}_p^{\,T})_i$ is

$$(\hat{\mathbf{c}}_p^{\,T})_i = (\mathbf{r}_p^{\,T})_i\, \mathbf{S}^{+} \tag{12}$$

It is often useful to include constraints, such as requiring all elements in **S** and $(\hat{\mathbf{c}}_p^{\,T})_i$ to

be greater than or equal to zero.

Multiple Linear Regression

When the sample spectra cannot be approximated as a simple sum of pure component spectra, either because some of the components are unknown or because Beer's law is inapplicable, indirect calibration in used. The basic model is

$$\mathbf{C} = \mathbf{R}\,\mathbf{P} + \mathbf{E}_C \tag{13}$$

where $\mathbf{E}_C$ is the error in the concentration matrix and $\mathbf{P}$ is the I by J matrix of coefficients, similar to $\mathbf{S}$. $\mathbf{C}$ may be any constituents, not just chemical concentrations. The equation is solved to minimize $\mathbf{E}_C$, and prediction is

$$(\hat{\mathbf{c}}_p^T)_i = (\mathbf{r}_p^T)_i\,\mathbf{P} \tag{14}$$

Since estimating $\mathbf{P}$ involves calculating the pseudoinverse of $\mathbf{R}_c$, J must be small. If the spectra originally contain a large number of wavelengths, there are two methods of simplifying the spectral data: selecting a few relevant wavelengths and factoring the whole spectrum.

Multiple linear regression (MLR), also known as inverse least squares[34] and the P-matrix approach[35], is an inverse least squares model that uses the spectral data from a small, selected set of wavelengths. The model is

$$\mathbf{c}_k^T = \mathbf{R}\,\mathbf{p}_k^T + \mathbf{e}_c \tag{15}$$

where $\mathbf{p}_k^T$ is the vector of regression coefficients for the k^{th} constituent and $\mathbf{e}_c$ is the error in the concentration matrix.

The most common method for choosing the wavelengths to use in the MLR model is to calculate the correlation coefficients between all wavelengths and the constituent of interest. The wavelength with the greatest correlation in chosen as the first wavelength for the model. The variance associated with the correlation is removed from the spectral

and constituent data and a second wavelength is chosen, and so on. Other methods also exist.

Principal Component Regression

Principal component regression (PCR)[36,37] uses the same fundamental definition as MLR but decomposes the full spectral matrix **R** into two factor matrices **T** and **P**,

$$\mathbf{R} = \mathbf{T}\,\mathbf{P} + \mathbf{E}_R \tag{16}$$

which can be calculated by singular value decomposition:

$$\mathbf{R} = \mathbf{V}\,\mathbf{S}\,\mathbf{U}^T + \mathbf{E}_R \tag{17}$$

where **V** is *I* by *A*, **S** is *A* by *A*, and $\mathbf{U}^T$ is *A* by *J*, and *A* is the number of factors (principal components). **T** and **P** are **VS** and $\mathbf{U}^T$, respectively. The matrix **T** contains "scores," linear combinations of concentration data, and **P** contains "loadings," linear combinations of spectral data. Scores and loadings are difficult to interpret in terms of the individual components. The concentrations can be estimated from the scores,

$$\mathbf{c} = \mathbf{T}\,\mathbf{q} + \mathbf{e}_c \tag{18}$$

$$\hat{\mathbf{c}}_p = \mathbf{R}_p\,\hat{\mathbf{P}}^T\,\hat{\mathbf{T}}_c^{+}\,\mathbf{c}_c \tag{19}$$

where **q** is the vector of coefficients that relates **c** to **T** and is estimated as $\hat{\mathbf{T}}_c^{+}\,\mathbf{c}_c$. If $\hat{\mathbf{c}}_p$ is not calculated, this method is known as principal component analysis (PCA) and does not require any constituent values. This method is useful as a classification technique, particularly when constituent values are unavailable.

Classification

When constituent data is discrete, such as the place of origin of the samples or "acceptable" and "unacceptable", classification algorithms are used. The most common is K Nearest Neighbors (KNN). The samples are treated as points in a multidimensional

space and their "nearness" to each other are calculated:

$$D_{ij} = \|\mathbf{r}_i - \mathbf{r}_j\| \quad (20)$$

where D_{ij} is the distance between samples *i* and *j*, and $\mathbf{r}_i$ and $\mathbf{r}_j$ are the spectral or score vectors for the two samples. It is assumed that samples within a class will be closer to each other than to samples in another class.

Like calibration, KNN classification requires a training set of samples whose classifications are known. However, there is no matrix of regression coefficients, an unknown sample is simply compared to all samples in the training set, one at a time. If $K = 1$, the unknown sample is assigned to the class of the training set sample that it is closest to. Otherwise the classifications of the *K* nearest training samples are considered.

The data used for KNN is often scaled (weighted) so that the variables which have the largest correlation to the classification are bigger than those which are less relevant. One common method of determining which variables are relevant is the variance weight,[38] which is the ratio of the intercategory variances to the sum of the intracategory variances. The equation is

$$w_{ab} = 2 * [(1/N_a)\Sigma x_a^2 + (1/N_b)\Sigma x_b^2 - (2/N_a N_b)\Sigma x_a \Sigma x_b] / [(1/N_a)\Sigma(x_a - x_{a,m})^2 + (1/N_b)\Sigma(x_b - x_{b,m})^2] \quad (21)$$

where N_a and N_b are the number of samples in classes *a* and *b*, *x* are the values of the variable in question, and $x_{a,m}$ is the mean of *x* for samples in class *a*.

RESULTS

Case Study

A case study is included here to illustrate typical results for shallow and full thickness burns. Patient #14 had a small scald burn on her foot. Hot water had run

down into her high-top boot, producing a shallow partial thickness burn at the top and a deep burn where the water pooled at the bottom. In the spectrum of the shallow partial thickness burn (Figure 2a) the oxy- and deoxy- hemoglobin bands (400-600 nm) are very intense, because the epidermis was absent and the wound was inflamed. In the near infrared region (700-1800 nm) there are three absorbance bands that arise from the overtones of O-H stretching modes of water (960, 1150, and 1450 nm). The discontinuity in the spectrum at 900 nm is an instrumental artifact, caused by a filter change.

The spectrum of the deep burn (Figure 2b) was markedly different. The baseline was considerably higher and the water bands in the near infrared were less intense. The cause of these differences is unknown. The 560 nm hemoglobin bands are also less intense, as there is less blood in the injured skin. All of the above had been expected. At 630 nm, however, the is an unanticipated band. The intensity of this band, evident as a shoulder on the oxy-/deoxy- hemoglobin peak, suggested that it was due to another form of hemoglobin. The band was attributed to the acid form of methemoglobin which has a band at 630 nm (Figure 1a). This compound is relatively well known and is present in normal subjects at the 0.5-1.0% level. Other hemoglobin derivatives may also be present in smaller quantities.

Principal Component Models

Raw Spectra

The spectra from all of the burn wounds are shown in Figure 3. Twelve spectra, acquired from discolored (black, brown, or green; n=10) and first degree (n=2) burns contain spectral features that are not relevant to the discrimination of shallow and deep burns. They were not included in any of the calibration models, to avoid making the models more complicated than necessary, but were included in predictions to

demonstrate that they would not be misclassified. These spectra are shown in Figure 3 and subsequent figures as dotted lines.

The spectral regions which correlate to burn depth were located by calculating the variance weights (Equation 21) for the absorbances at each wavelength (Figure 4). There is some correlation between 550 and 580 nm, but little or none (variance weight = 2) anywhere else. This indicates that the hemoglobin absorbances (550-580 nm) have some correlation to burn depth, which is in accord with one of the fundamental tenets of clinical assessment, that the darker pink a wound is, the more likely it is to be shallow. The low correlation in other portions of the spectra indicates that the baseline offsets are unrelated to burn depth and are probably caused by irreproducibility in the source / sample / detector geometry.

Since the major spectral features do not correlate strongly to burn depth, the spectra were analyzed by Principal Component Analysis (Equations 16-19) to locate minor features which might be more relevant. The spectra would be expected to display at least four major types of variation, corresponding to baseline offsets, multiplicative factors (path length and total blood concentration), oxygenation of the blood, and methemoglobin concentration. Minor variations, representing minor chemical components or spectral non-linearities would also be expected. The first four principal component loadings (spectral domain, Figure 5a,b) show that there are indeed at least four significant types of orthogonal spectral variance. The next four (Figure 5c,d) model only a small amount of the total variance. It is possible, but unlikely that these later factors are significant.

The principal component scores (concentration domain, Figure 6) show that the first two factors, are dominated by irrelevant effects of sample/instrument geometry. Similar effects have been observed in the diffuse reflectance spectra of other irregularly-shaped samples.[39] The third and fourth principal components, however, are correlated

to burn depth. The variance weights for the first eight principal components are 2.3, 2.5, 2.7, 3.2, 2.5, 2.3, 2.0, and 2.0.

The distinction between "shallow" and "deep is a somewhat arbitrary division of a continuous variable, the fraction of dermis destroyed. It might be expected that in a multidimensional space, the scores for shallow burns might be located on one side and those for deep burns on the other, with the borderline injuries inbetween (Figure 6b). Shallow burns would most likely be closest to other shallow burns, etc., so KNN should give reasonable results. The KNN algorithm in Pirouette[40] successfully classified 100 (91%) of the 110 spectra, using 4 principal components. The optimal number of neighbors to consider was found to be 2. Cross validation, leaving out one patient's spectra each time (MATLAB program written by the author), successfully classified 101 (92%), using 6 principal components and considering 3 neighbors.

Assuming that there is only one continuous variable which relates to burn depth, another possible method of classification is to define a multidimensional plane between the two classes. All scores on one side of the plane should represent shallow burns, and all scores on the other side should represent deep injuries. This plane may be found by rotating the axes so that the first axis corresponds to the direction of the variance in the data which most clearly distinguishes between the two classes. The discrimination plane is then perpendicular to the first rotated axis.

The algorithm used for single-plane discrimination involved 5 steps. The first step was to mean-center[*39] the scores. Then the mean-centered scores were range scaled[*39] and feature weighted,[*39] according to the variance weight. The scaled data was then rotated, two dimensions at a time, starting with those which have the greatest variance weights. The best rotation was defined as that which produced the largest variance weight for the first of the two dimensions. Once the best rotation was found, the

discrimination plane was defined perpendicular to the first axis, located so that the number of misclassified calibration samples was minimized. The samples were classified according to which side of the discrimination plane their rotated scores were located. The MATLAB code for these programs are in Appendix A.

The scores, rotated in the first four dimensions, are shown in Figure 7. The discrimination plane is also shown, projected as a line. All but 7 of the samples are correctly classified by this plane. Including more than four dimensions does not improve classification, since only the first four principal components contain much relevant information. Cross validation, using 4 principal components correctly classified 102 (93%). The single-plane discrimination is slightly better than KNN because only one dimension contains relevant information. The model is simpler and less influenced by any single calibration sample.

The loadings, rotated in the same manner (Figure 8), show that there is a strong positive correlation between the absorbance at 630 nm and the depth of the burn. This is probably due to the absorbance of methemoglobin which appears to be characteristic of deep burns. There is also a strong negative correlation at 570 nm, where oxyhemoglobin absorbs. It is reasonable to assume that the more healthy, oxygenated hemoglobin a wound contains, the more likely it is to heal quickly. The first rotated loading is small for the wavelengths 650-700 nm indicating that this region, which contains little hemoglobin absorbance, is not useful for prediction. This further supports the previous results indicating that the baseline offsets are unrelated to burn depth. Subsequent rotated loadings (not shown) are not correlated to burn depth (variance weights < 2.2).

Baseline subtracted spectra

Since the baseline offsets are useless, they can be removed without losing information, approximating the baseline by the apparent absorbance at 700 nm (Equation 7, J_b = 700 nm). Among the resulting spectra (Figure 9) the spectral differences between the two classes are more obvious. The intensity of the hemoglobin absorbance (520-580 nm) is, on the average, greater for shallow injuries than for deep, but this variable alone is insufficient for diagnosis. Considering only the intensity of the absorbance, what the eye sees, only 69% of the injuries, at best, could be correctly classified. Clinical assessment considers a few other variables and is potentially more accurate.

Since the variance due to the offsets has been removed, fewer principal components should be needed to describe the data set. The first four loadings (Figure 10) are similar to those from the raw spectra (Figure 5). The subsequent loadings, however, contain more noise. The second and third principal components are most highly correlated (Figure 11), rather than the third and fourth (Figure 6), and the variance weights for the principal components are greater, 2.5, 4.6, 2.9, and 2.2 for the first four. Prediction results from KNN and single-plane discrimination are not significantly better, but the model is simpler.

Normalized spectra

Although the amount of blood visible in a wound is a good indication of its viability, it is an unreliable indicator. Edema (inflammation) and hematoma (bruising) both increase the amount of blood without increasing the healing potential. In this study, the diagnostic errors made by the physicians were caused either by injuries that were outside the range of their experience, such as an unusual chemical burn, or by deep injuries that appeared pink instead of white. To correctly diagnose these wounds it is helpful to focus on the

second factor which relates to burn depth, the methemoglobin content.

To remove the variance caused by variable amounts of blood in the skin, the spectra were normalized to the maximum of the average spectrum (570 nm was chosen). The normalization equation is

$$(\mathbf{r}_i)_{\text{normalized}} = (\mathbf{r}_i)_{\text{baseline subtracted}} / r_{i,570nm} \quad (22)$$

where $r_{i,570nm}$ is the apparent absorbance of the i^{th} spectrum at 570 nm. The methemoglobin absorbance at 630 nm is clearly visible in the normalized spectra (Figure 12).

The removal of the multiplicative factors is inaccurate since this normalization is somewhat simplistic, so the rank of the spectral data set does not decrease. But since the data is simplified, the correlation to burn depth increases (Figure 13). The loadings (Figure 14) are similar to those of the baseline-corrected spectra (Figure 10), but the scores of the first two principal components (Figure 15) are more highly correlated. The variance weights for the first four principal components are 3.5, 5.3, 2.8, and 2.2. Prediction results are nearly identical to those from the baseline-corrected data.

Hemoglobin Spectra Model

Single Layer Model

The above results suggest that there is a single spectral feature or single combination of interrelated features which is indicative of the depth of a burn wound. Further, in the normalized spectra, the 630 nm absorbance, attributed to the acid form of methemoglobin, correlated to burn depth. This suggests that the concentration of acidic methemoglobin in the skin, relative to the total blood volume, is proportional to the amount of tissue damage and, hence, to the length of time required for healing. Unfortunately, there is no way to test this hypothesis directly. Even if the patients

consented to having skin samples removed for analysis, conventional methods of hemoglobin speciation are not applicable to solid tissue samples.

One alternative is to attempt to reproduce the observed reflectance spectra, starting from the spectra of pure hemoglobins. Assuming that (a) the particles in the skin scatter light isotropically, (b) the hemoglobin is uniformly distributed, (c) there is no specular reflectance or stray light, and (d) the only absorbing compounds in the skin are hemoglobins, then the reflectance spectra of the skin could be modeled as a linear sum of pure hemoglobin spectra, using Classical Least Squares (Equations 9-12). None of the assumptions are actually true and the hemoglobins used to acquire the basis spectra were not 100% pure, so the model is not expected to fit the data precisely. The spectra of the hemoglobins (the matrix **S**) are shown in Figure 16, including oxyhemoglobin, deoxyhemoglobin, acid methemoglobin, base methemoglobin, and a baseline. The spectra were fit to a reflectance spectrum of a burn wound, and a new spectrum was reconstructed from the estimated hemoglobin concentrations. This was repeated for all burn spectra.

Two examples are shown in Figure 17. The reconstructed spectra are not exactly the same as the measured spectra, since the assumptions are incorrect. This simplistic model does, however, give an estimate of methemoglobin in a burn, information which has previously been unavailable. The resulting predictions are less accurate (79%) than those from the empirical PCA models, indicating that the methemoglobin concentration alone is insufficient to predict healing or that the fitting errors were too large, probably both. However, the success of this model in discrimination does strongly support the hypothesis that oximetric information correlating to burn depth can be obtained from the spectra.

Two Layer Model

Of the assumptions used in the above model, two are approximately true, one might be true, and one is definitely false. The hemoglobin is not distributed homogeneously; in most cases there is a layer of bloodless, dead tissue (eschar) at the surface. This layer reflects incident light, reducing the amount that interacts with the blood beneath. The reflectance from a non-absorbing layer is dependent on light scattering and is a function of wavelength.

If the amount of light of wavelength j, reflected from the sample is I_j, and the total incident light is $I_{0,j}$, then the instrument response ($R_{obs,j}$) is

$$R_{obs,j} = I_j / I_{0,j} \tag{23}$$

$$R_{obs,j} = (I_{s,j} + I_{r,j}) / (I_{s0,j} + I_{r,j}) \tag{24}$$

where $I_{r,j}$ is the intensity reflected from the non-absorbing eschar layer, $I_{s0,j}$ is the intensity of the light that passes through the first layer and enters the second, blood-filled layer, and $I_{s,j}$ is the intensity of the light returning from the second layer. The fraction of the incident radiation that would be diffusely reflected from the second layer, if there were no specular reflectance and if the first layer were removed, is $R_{s,j}$,

$$R_{s,j} = I_{s,j} / I_{s0,j} \tag{25}$$

and is related to the absorbance of the blood in the second layer ($A_{s,j}$),

$$A_{s,j} \approx \log(1/R_{s,j}) \tag{26}$$

It can be estimated from the instrument response:

$$R_{s,j} = (I_{0,j} R_{obs,j} - I_{r,j}) / (I_{0,j} - I_{r,j}) \tag{27}$$

$$R_{s,j} = (T_{obs,j} - S_j) / (1 - S_j) \tag{28}$$

$$S_j = I_{r,j} / I_{0,j} \tag{29}$$

if S_j is known.

For the burn spectra, S is not known. Instead, S was approximated by a second

order polynomial, a function of the wavelength (λ):

$$S \approx s_0 f(\lambda^0) + s_1 f(\lambda^1) + s_2 f(\lambda^2) \quad (30)$$

R_s should be, approximately, the product of the transmittances (T_k) of the hemoglobin species (k) times their concentrations (c_k).

$$R_s \approx {}_k\prod (c_k T_k) \quad (31)$$

And therefore

$$(T_{obs,j} - S_j) / (1 - S_j) \approx {}_k\prod (c_k T_k) \quad (32)$$

There are $3+k$ variables which must be solved simultaneously (s_0, s_1, s_2, c_1, c_2, ... c_k) by using a non-linear curve fitting algorithm and minimizing the spectral fitting error:

$$\text{error} = (T_{obs,j} - S_j) / (1 - S_j) - {}_k\prod (c_k T_k) \quad (33)$$

The Gauss-Newton algorithm supplied by Mathworks[41], gave satisfactory results, under the following constraints:

$$c_k \geq 0 \quad (34)$$

$$0 \leq S_j \leq 1 \quad (35)$$

The reconstructed spectrum (A_{obs}) is then

$$T_{obs,j} = T_{s,j} (1-S_j) + S_j \quad (36)$$

$$A_{obs,j} \approx - \log(T_{obs,j}) \quad (37)$$

The transmission spectra of hemoglobins and the functions $f(\lambda^0)$, $f(\lambda^1)$, and $f(\lambda^2)$ are shown in Figure 18. The reconstructed spectra for the two examples are shown in Figures 19 and 20. In general, the fit was not improved if S was assumed to be 0th order with respect to wavelength ($s_1 = 0$ and $s_2 = 0$). When S was 1st order, there was significant improvement; nearly all of the systematic distortion was accounted for. Adding the 2nd order improved some of the more unusual spectra, but generally had little effect on the "typical" spectra. The 1st order model indicated that deep burns usually have more than 9% acid methemoglobin (Figure 21) and correctly classified 90% of the injuries.

Skin Temperature Model

In the second year, spectra were acquired from the forearms of healthy volunteers. Their skin temperature was varied from 9 to 35 °C and measured with a thermistor at the surface. The spectra, after second derivative transformation, were analyzed by Multiple Linear Regression (Equations 13-15) and were found to correlate to the skin temperature (correlation coefficient R = 0.982), with a standard error of prediction of 1.4 °C. This experiment is described in the previous report.[42] The equation was

$$t = 22.7 + (1.21\text{x}10^6)\, r''_{1015nm} - (1.44\text{x}10^6)\, r''_{1073nm} - (3.85\text{x}10^5)\, r''_{1156nm} \qquad (38)$$

where r''_{1015nm} is the second derivative (Equation 8, gap=23) at 1015 nm and t is the temperature in °C.

The model for estimating skin temperature in normal skin was used to estimate the temperature of the burn wounds. The results suggest that deeper burns are cooler than shallow burns (Figure 23). The average estimated temperatures were 32 ± 7 and 27 ± 7 for shallow and deep burns ($P<0.01$). Thermography, using emitted infrared light, has also shown that deep burns are cooler than shallow,[11,12] but that such measurements are extremely sensitive to cooling caused by evaporation of surface water. NIR reflectance should be less sensitive to surface effects, since it measures that temperature within the skin and below it. The model used here is not optimal; it is derived from healthy skin. A more accurate model could be obtained empirically, if the temperatures of wounds could be measured by a contacting or invasive probe, or theoretically, if the spectral non-linearities were better understood.

Although several features in the NIR spectra, including water temperature correlated to burn depth, none were as useful as the hemoglobin bands, nor did they improve prediction. It is likely that there is still much useful information in these spectra, but in the absence of physiological reference data, this information could only be extracted by

rigorous application of diffuse reflectance theory.

BDI and IBDI Simulations

Now it is possible to explain the predictive ability of the old Burn Depth Indicators (imaging and non-imaging). Both instruments used baseline-subtracted, single-wavelength normalized data. The baseline offsets were approximated by the instrument response of the NIR LED (880 nm) or filter (880-1100 nm) and the remaining data was normalized to the response of the Green (560 nm). The methemoglobin concentration was then, inadvertently, approximated by the normalized response of the Red (640 nm). The exact mathematics are slightly different, because instruments used the instrument response (R) rather that $\log(1/R)$, but the principle is the same.

In order to compare the prediction results from our spectrophotometer with predictions from the Burn Depth Indicator (BDI) and the Imaging Burn Depth Indicator (IBDI) built previously, the BDI and IBDI responses were simulated from our spectra. The emission spectra of the light emitting diodes (LED's) in the BDI were simulated as Gaussian-shaped peaks with maxima at 550, 640, and 880 nm and band widths (fwhm) of 70 nm.[*21,*22] The spectra of the IBDI filters (Figure 24b) were obtained from the literature.[*20] The responses for the near infrared LED and filter are somewhat uncertain, because our spectral data between 750 and 890 nm is unreliable and was not used. The simulated results (Figures 25a and 25b), however, are reasonably close to those obtained in previous work.[*19,*22] For the few wounds for which IBDI images were acquired, the simulated results agree with the images. The burn sites used in this study seem to have a slightly wider range, both for the Red/NIR and Green/NIR ratios, than those used in previous studies, which is consistent with our attempt to select the widest variety of injuries. The accuracy of the BDI and IBDI simulations for prediction burn depth was

about 77 and 79%, respectively. VanLiew and Moore reported 79 and 84% accuracies for different sets of indeterminate burns for the two instruments.[*18,*20]

Proposed Model for New Imaging-Burn-Depth-Indicator

These results show that the model used for the Burn Depth Indicators was essentially sound and from the perspective of burn physiology, basically correct, though its explanation was erroneous. The choice of wavelengths, however, could be substantially improved. First, the filter originally selected for baseline subtraction (880-1100 nm) measures a large absorbance band at 970 nm (Figure 24) as well as the offsets. This band arises, in part, from the water in and on the skin. The water absorption is variable but not well correlated to burn depth. The 880-1100 nm filter also measures the absorbances of hemoglobins (Figure 1b), but the path length in this region is much longer than in the visible region. It is uncertain whether the blood in the volume sampled is representative of the blood in the skin or primarily below the skin. Furthermore, the BDI and IBDI simulations produced comparable results, in spite of the fact that the wavelength ranges used for baseline correction were significantly different. Therefore, little relevant information is lost and some interference is avoided by moving the baseline-correction filter to 650 or 700 nm, where the absorbances are significantly lower.

Second, the normalization filter could be narrowed and shifted to produce a more reliable response. There is a pronounced, non-linear distortion of the spectra which affects the 550-580 nm region where the hemoglobin absorbance is particularly strong. In the spectra of whole blood (Figure 1a), the two oxyhemoglobin absorption bands (535 and 570 nm) have similar intensities. In the burn spectra, however, the 535 nm band is decreased relative to the 570 nm band, and the degree of distortion is unrelated to burn

depth. The distortion is probably caused by scattering, and scattering is highly wavelength dependent. Therefore, the scattering at 630 nm is likely to be more similar to that at 570 nm than 535 nm, and the former should give a more accurate normalization for the 630 nm methemoglobin band. Simulations of fixed-filter instruments using various possible normalization filters confirm this. The normalization LED for the BDI had a 80 nm band width and was at 560 nm, sampling both oxyhemoglobin bands equally. The filter in the IBDI at 540 nm was worse, sampling only the most distorted portion of the oxyhemoglobin spectrum. A filter with a narrower band width, 30 nm or less, and located at 570 nm should give a more reliable normalization.

Third, the methemoglobin filter should be optimized. The filter used previously had a 80 nm band width and was centered at 640 nm. The methemoglobin absorbance peak is at 630 nm, and for the normalized spectra, the wavelength that correlates most to burn depth is 625 nm (Figure 13). The band width of the methemoglobin band is approximately 40 nm. A narrower filter, 40 nm fwhm or less, centered at 630 nm should give more precise estimates of methemoglobin absorbance.

One possible filter selection might include three 20-nm band pass filters at 650, 570, and 630 nm. If the apparent absorbances (log (1/R)) of the three filters are A_{650}, A_{570}, and A_{630} respectively (Figure 26), then the burn depth (D) is estimated by

$$D = (A_{630} - A_{650}) / (A_{570} - A_{650}) \quad (39)$$

The discrimination point, calculated the same way as the discrimination plane for the rotated PCA scores, was found to be 0.104. Injuries for which D is greater than 0.104 were deep and the rest were shallow. One hundred one (92%) of the sites were correctly classified by this model, and 97 (88%) were classified during cross validation. This model was significantly more accurate (88%) than the IBDI simulation (79%) for the 104 sites simulated ($P<0.06$ for paired data). Small variations in the band width or mean

wavelength of the filters do not significantly affect prediction ability, indicating that an instrument using this algorithm would be relatively tolerant of manufacturing variations.

Although binary predictions (shallow or deep) are convenient, it is often useful to rank injuries on a continuous scale, so that the size of the burn and patient comfort often may be weighted against the estimated healing potential. The proposed algorithm can be used to produces a continuous scale (D) as well as binary predictions. For sites which were known to have healed in the third and fourth weeks post burn, there is roughly a linear correlation between instrument response and healing time (Figure 27). The estimated number of days required for healing (H) is

$$H = 30\,D + 15 \tag{40}$$

This relationship is not applicable to sites which heal in less than two or more than four weeks, but such information would rarely be important in management decisions.

For sites which heal between 14 and 28 days, the error in this model (± 3 days) is comparable to the uncertainty of the reference method (± 2 days). Whether or not a wound was healed (entirely reepethilialized) is difficult to determine precisely. Even among the Burn Center staff, opinions differed by a day or two. For wounds whose outcomes were described by patients over the phone or extrapolated from the nurses' last observations, the uncertainty was about ±3 days.

CONCLUSIONS

With the LT spectrometer we are able to observe absorbance bands from most of the major constituents of skin. The instrument is sensitive enough to monitor changes as small as those induced by only a few degrees elevation in surface temperature. The techniques used are completely non-invasive, non-contacting, and non-destructive and require only a few minutes, making them suitable for use on burn patients.

In spite of the non-linear effects of light scattering and multiple layers, hemoglobin speciation can be estimated from visible reflectance measurements of burn wounds. Further, these estimates correlate to the depth of the injury. Severely elevated levels of methemoglobin have been observed in deep partial thickness and full thickness burns. This suggests that the Imaging Burn Depth Indicator estimates burn depth by analyzing the small color changes caused by the presence of methemoglobin. The IBDI, initially designed to measure deoxyhemoglobin, can be significantly improved by optimizing its filters to detect methemoglobin. The resulting instrument would be fast, accurate, non-invasive, and non-contacting and could produce a map of a wound, color-coded to indicate healing potential. This improved instrument could be used as a practical guide for burn treatment decisions and may assist in the study of burn physiology.

Bibliography

1. Johnson, C.L.; O'Shaughnessy, E.J.; Ostergren, G. *Burn Management*, **1981**, Raven Press, N.Y., NY.

2. Engrav, L.H.; Heimbach, D.M.; et. al. *J Trauma*, **1983**, *23*, 1001-1004.

3. Heimbach, D.M.; Engrav. L.H. *Surgical Management of the Burn Wound*, **1984**, Raven Press, N.Y., NY, Ch.1.

4. Godina, M.; Derganc, M.; Brcic, A. *Burns*, **1978**, *4*, 92-96.

5. Panke, T.W.; McLeod, C.G. *Pathology of Thermal Injury: A Practical Approach*, **1985**, Grune & Stratton, N.Y., NY.

6. Gürsu, K.G. *Burns*, **1978**, *4*, 97-103.

7. Patey, D.H.; Scarff, R.W. *Brit J Surg*, **1944**, *32*, 32-35.

8. Davies, M.R.Q.; Adendorff, D.; Rode, H.; van der Riet, R. leS. *Burns*, **1980**, *6*, 156-159.

9. Bennett, J.E.; Dingman, R.O. *Plastic and Reconstructive Surgery*, **1957**, *20*, 261-272.

10. Bauer, J.A.; Sauer, T. *Burns*, **1989**, *15*, 49-51.

11. Cole, R.P; Jones, S.G.; Shakespeare, P.G. *Burns*, **1990**, *16(1)*, 60-63.

12. Newman, P; Pollock, M.; Reid, W.J.; James, W.B. *Burns*, **1981**, *8*, 59-63.

13. Bardakjian, V.B.; Kenney, J.G.; et. al. *J Burn Care Rehab*, **1988**, *9(1)*, 63-65.

14. Green, M.; Holloway, G.A.; Heimbach, D.M. *J Burn Care Rehab*, **1988**, *9(1)*, 57-62.

15. O'Reilly, T.J.; Spence, R.J.; Taylor, R.M.; Scheulen, J.J. *J Burn Care Rehab*, **1989**, *10(1)*, 1-6.

16. Anselmo, V.J.; Zawacki, B.E. *Proceedings of the Society of Photo-Optical Instrumentation Engineers, Quantitative Imagery in the Biomedical Sciences -- II*, **1973**, *80*, 181.

17. Anselmo, V.J.; Zawacki, B.E. *Annals of Biomedical Engineering*, **1977**, *5*, 179-193.

18. Heimbach, D.M.; Afromowitz, M.A.; Engrav, L.H.; Marvin, J.A; Perry,B. *J Trauma*, **1984**, *24(5)*, 373-378.

19. Afromowitz, M.A.; Van Liew, G.S.; Heimbach, D.M. *IEEE*, **1987**, *BME-34(2)*, 114-126.

20. Afromowitz, M.A.; Callis, J.B.; Heimbach, D.M.; DeSoto, L.A.; Norton, M.K. *IEEE*, **1988**, *BME-35(10)*, 842-849.

21. DeSoto, L.A. *A Burn Depth Imaging System* **1986**, University of Washington M.S. thesis.

22. Moore, M.K *A Clinical Evaluation of the Imaging Burn Depth Indicator*, **1987**, University of Washington, MS thesis.

23. Van Liew, G.S. *A Statistical and Optical Analysis of Light Reflectances of Burn Injured Skin*, **1984**, University of Washington, M.S. thesis.

24. Nelcor Inc., Hayward, CA.

25. Shapiro, B.A.; Cane, R.D. *Crit Care Med*, **1989**, *17*, 573-581.

26. Wyatt, J.S.; Cope, M.; et.al. *Lancet*, **1986**, 1063-66.

27. Cope, M.; Delpy, D.T. *Med & Biol Eng & Comput*, **1988**, *26*, 289-294.

28. Barbour, R. *Instrumentation Research*, **1985**, *March*, 59-64.

29. Hampson, N.B.; Piantadosi, C.A. *J Appl Physiol*, **1988**, *64(6)*, 2449-2457.

30. *Near-Infrared Technology in the Agricultural and Food Industries*, **1987**, William, P.; Norris, K., Eds.; American Association of Cereal Chemists, St.Paul, MN.

31. Stark, E.; Luchtir, K.; Margoshes, M. *Appl Spec Rev*, **1986**, *22(4)*, 335-399.

32. LT Industries, MD.

33. Strang, G. *Linear Algebra and Its Applications* **1980**, Academic Press: Florida, 137-145.

34. Thomas. E.V.; Haaland, D.M. *Annal. Chem.* **1990**, *62*, 1091-1099.

35. Brown, C.W.; Lynch, P.F.; Obremski, R.J.; Lavery, D.S. *Anal. Chem.* **1982**, *54*,

1472-1479.

36. Haaland, D.M.; Thomas, E.V. *Anal. Chem.* **1988**, *60*, 1193-1202.

37. Wold, S.; Esbensen, K.; Geladi, P. *Chemom Intell Lab Syst* **1987**, *2*, 37-52.

38. Sharaf, M.A.; Illman, D.L.; Kowalski, B.R. *Chemometrics* **1986**, John Wiley & Sons: New York.

39. Balkenhol, M.B. *NIR and Visible Spectroscopy of Irregular Solids*, **1992**, University of Washington, PhD thesis.

40. "Pirouette", Infometrics, Seattle, WA.

41. MATLAB, The Math Works, Inc., Cochituate Place, 24 Prime Park Way, Natick, MA 01760, 1990.

42. Afromowitz, M.A.; Callis, J.D. *Spectroscopy of Burn Wounds* **1991**, Annual report to the U.S. Army Medical Research & Development Command, Contract #DAMD17-88-C-8125.

Appendix A
MATLAB Code for Rotation and Single-Plane Discrimination

```
function [Xmean,Scale,Rota] = spinc(X,C,Options)
% X = all data (samples by variables, more samples than variables)
% C = class vector, containing 1's and 2's only, 0's for ignored data
%OUTLINE
% mean center
% scale
% rotate
%SUBROUTINES NEEDED
% std, varwt, fisherwt
%OPTIONS
% 1 scale (Range, Auto, Variance, Fisher, none)
% 2 rotation steps
% 3 number of rotated variables to calculate
%function [Xmean,Scale,Rota] = spinc(X,C,Options)


%%%%%%%%%%%%%%%%%%%%%%%%%%%%%%%%%%%%%%%%%%%%%%%%%%%%%%%%%%%%       SETUP
%%%%%%%%%%%%%%%%%%%%%%%%%%%%%%%%%%%%%%%%%%%%%%%%%%%%%%%%%%%%
%************************************************************ CHECK SIZES *****
%CHECK SIZES
 [m,n] = size(C);
   if m~=1 & n~=1,  error('Rotation: Too many constituents.'),  end
   if n>m,  C=C';  [m,n]=size(C);  end
 [np,nv] = size(X);
   if np~=m & nv~=m, error('Rotation: Incompatible matrices'), end
   if nv==m,  X=X';  [np,nv]=size(X);  end
 clear m n

 if any(C~=1 & C~=2 & C~=0),  error('Rotation:  Bad constituent values.'),  end
 n1 = find(C==1);
   if length(n1)<2,  error('Rotation: Too few of class #1'),  end
 n2 = find(C==2);
   if length(n2)<2,  error('Rotation: Too few of class #2'),  end

 if ~any([1 2 3 4 5] == Options(1)),
   error('Rotation: Not a valid scaling option.')
 end
 if length(Options)<3, Options(3)=nv-1; end
 if Options(3)>nv-1,    Options(3)=nv-1; end

%************************************************************ SETUP MATRICES *****
%SETUP MATRICES
 PhiStepSize = 1 / Options(2);
 Rota = eye(nv);                       %Main rotation matrix
 Cycle = 0;


%%%%%%%%%%%%%%%%%%%%%%%%%%%%%%%%%%%%%%%%%%%%%%%%%%%%%%%%%%%%
%                  PREPROCESS DATA
%%%%%%%%%%%%%%%%%%%%%%%%%%%%%%%%%%%%%%%%%%%%%%%%%%%%%%%%%%%%
%************************************************************ MEAN-CENTER *****
%MEAN-CENTER
 Xmean = mean(X);
 Data  = X - ones(np,1)*Xmean;
```

```
%************************************************************** SCALE *****
%SCALE (Sharaf,Illman,Kowalski; "Chemometrics", p.193)
 if Options(1) == 1, %_____ Range scaling ____
  for i=1:nv, Scale(i) = 1 / max(abs(Data(:,i))); end
 elseif Options(1) == 2, %_____ Autoscaling ____
  for i=1:nv, Scale(i) = 1 / std(Data(:,i)); end
 elseif Options(1) == 3, %_____ Variance weights ____
  for i=1:nv, DataTmp(:,i)=Data(:,i)/max(abs(Data(:,i))); end
  [Scale] = varwt(DataTmp,C);
  for i=1:nv, Scale(i)=Scale(i)/max(abs(Data(:,i))); end
 elseif Options(1) == 4, %_____ Fisher weights ____
  for i=1:nv, DataTmp(:,i)=Data(:,i)/max(abs(Data(:,i))); end
  [Scale] = fisherwt(DataTmp,C);
  for i=1:nv, Scale(i)=Scale(i)/max(abs(Data(:,i))); end
 elseif Options(1)==5,
  %no scaling
 end

 for i=1:nv,  Data(:,i)=Data(:,i)*Scale(i);  end

%%%%%%%%%%%%%%%%%%%%%%%%%%%%%%%%%%%%%%%%%%%%%%%%%%%%%%%%%%%%%%%%%%%
%                ROTATE (two vectors at a time)
%%%%%%%%%%%%%%%%%%%%%%%%%%%%%%%%%%%%%%%%%%%%%%%%%%%%%%%%%%%%%%%%%%%
for var1 = 1:Options(3),
for var2 = (var1+1):nv,
  %************************************************ TWO-VECTOR SUB-MATRICES *****
  %Choose vectors
   Data2 = Data(:,[var1,var2]);
   Rota2 = Rota(:,[var1,var2]);
   Axis  = sqrt(2) * [-1 1 -1 1] * max(max((Data2)));
  %************************************************************ ROTATE (loop) *****
  %Spin about [0 0]
  for phistep=1:Options(2),
    %++++++++++++++++++++++++++++++++++++++++++++++++++++++++++ Rotation Angle
    %Rotate data
     phi = phistep * PhiStepSize * (2*pi);
     rot = [cos(phi), -sin(phi); sin(phi), cos(phi)];
     data = Data2 * rot;
     rota = Rota2 * rot;
    %++++++++++++++++++++++++++++++++++++++++++++++++++++++ Distance Between Classes
    %Distance between classes
     [d,sign] = varwt(data(:,1),C);
     if sign == '-', d = -d; end
     dist(phistep) = d;
  end %for phistep
  %************************************************** FIND MAXIMUM ANGLE *****
  %Maximize distance
    %++++++++++++++++++++++++++++++++++++++++++++++++++++++++++++++++++ Angle
    maxphi = find( dist == max(dist) );
     if length(maxphi) > 1,  maxphi = maxphi(1);  end
    phi = maxphi * PhiStepSize * (2*pi);
    rot = [cos(phi), -sin(phi); sin(phi), cos(phi)];
   %************************************************** NEW SUB-MATRICES *****
   %New sub-matrices
    %++++++++++++++++++++++++++++++++++++++++++ New Matrices +++++
    data = Data2 * rot;
    rota = Rota2 * rot;
    Data(:,[var1,var2]) = data;
    Rota(:,[var1,var2]) = rota;
 disp(['Rotation: Finished variables ',int2str(var1),' and ',int2str(var2)])
end %for var2 = (var1+1):nv
end %for var1 = 1:(nv-1)
```

```
function [DataNew] = spinp(Xmean,Scale,Rota,Xp)
%function [DataNew] = spinp(Xmean,Scale,Rota,Xp)

[np ,nv] = size(Xp);

Data  = Xp - ones(np,1)*Xmean;
for i = 1:nv,  Data(:,i) = Data(:,i)*Scale(i);  end
  Data = Data * Rota;
for i = 1:nv,  Data(:,i) = Data(:,i)/Scale(i);  end
DataNew = Data  + ones(np,1)*Xmean;
```

```
function [discPoint] = disc(D,C);
% DISCc.m
% Finds the most discriminating point to separate two classes
% M.R.Balkenhol, 1/12/92
%
% D = data in two columns, column 1 is for discriminating
% C = class vector, 1's and 2's only
%
% minE  = best point (index and data value)
% E     = number of misclassifications [index, class1, class2, both classes]
%
%function [discPoint] = disc(D,C);


%%%%%%%%%%%%%%%%%%%%%%%%%%%%%%%%%%%%%%%%%%%%%%%%%%%%%%%%%%%%%%%            INPUT and
SETUP
%%%%%%%%%%%%%%%%%%%%%%%%%%%%%%%%%%%%%%%%%%%%%%%%%%%%%%%%%%%%%%
minD = min(D(:,1));
maxD = max(D(:,1));
maxi = 300;
Error  = 999*ones(maxi+1,1);
Error2 = 999*ones(maxi+1,1);
Index  = zeros(maxi+1,1);

%%%%%%%%%%%%%%%%%%%%%%%%%%%%%%%%%%%%%%%%%%%%%%%%%%%%%%%%%%%%%%
%               LOCATION OF MOST DISCRIMINATING POINT
%%%%%%%%%%%%%%%%%%%%%%%%%%%%%%%%%%%%%%%%%%%%%%%%%%%%%%%%%%%%%%
%************************************************** Fewest Mispredictions *****
for i=1:maxi,
 j = i*(maxD-minD)/maxi + minD;
 e1 = sum( D(:,1)>=j & C==1 );
 e2 = sum( D(:,1)< j & C==2 );
 Error(i) = e1 + e2;
end

[minEs] = min(Error);
minIs = find(Error==minEs);

%****************************************** Smallest Sum-of-Squares Error *****
I=min(minIs) : max(minIs);
for i=I,
 j = i*(maxD-minD)/maxi + minD;
 n1 = find( D(:,1)>=j & C==1 );
 n2 = find( D(:,1)< j & C==2 );
 Error2(i) = sum(  ( D([n1;n2],1) - j ).^2  );
end

[minE,minI] = min(Error2);
 n = length(minE);
 if n > 1,  minE = minE( round(n/2), : );  end

discPoint = minI*(maxD-minD)/maxi + minD;
```

```
function [Cest,ep] = discp(disc,Dp,Cp);
% DISCp.m
% Sorts a predictions set (Class1 < disc, Class2 > disc)
% M.R.Balkenhol, 1/12/92
%
% Dp = data in two columns, column 1 is for discriminating
% Cp = class vector, 1's and 2's only (optional)
%
% disc = discriminating point, minE(1,2) from disc.m
%
%function [Cest] = discp(disc,Dp,Cp);


%%%%%%%%%%%%%%%%%%%%%%%%%%%%%%%%%%%%%%%%%%%%%%%%%%%%%%%%%%%%%%%%%%%%%%          INPUT and
SETUP
%%%%%%%%%%%%%%%%%%%%%%%%%%%%%%%%%%%%%%%%%%%%%%%%%%%%%%%%%%%%%%%%%%%%%%
[np,nv] = size(Dp);


%%%%%%%%%%%%%%%%%%%%%%%%%%%%%%%%%%%%%%%%%%%%%%%%%%%%%%%%%%%%%%%%%%%%%%
%          SORTING DATA POINTS with respect to DISC
%%%%%%%%%%%%%%%%%%%%%%%%%%%%%%%%%%%%%%%%%%%%%%%%%%%%%%%%%%%%%%%%%%%%%%
for i=1:np,
  if Dp(i,1) < disc,
    Cest(i) = 1;
  elseif Dp(i,1) > disc,
    Cest(i) = 2;
  else
    Cest(i) = 0;
  end
end
Cest = Cest';


%%%%%%%%%%%%%%%%%%%%%%%%%%%%%%%%%%%%%%%%%%%%%%%%%%%%%%%%%%%%%%%%%%%%%%
%              DISPLAY (if Cp exists)
%%%%%%%%%%%%%%%%%%%%%%%%%%%%%%%%%%%%%%%%%%%%%%%%%%%%%%%%%%%%%%%%%%%%%%
if nargin > 2,
  errors = find( Cest ~= Cp );
  plot(find(Cest==1), Dp(Cest==1,1), 'c6+',...
       find(Cest==2), Dp(Cest==2,1), 'rx',...
       [1 np], [disc disc], 'b:',...
       errors, Dp(errors,1), 'c5o')
  ep = length(errors);
end
```

Spectra of Hemoglobin

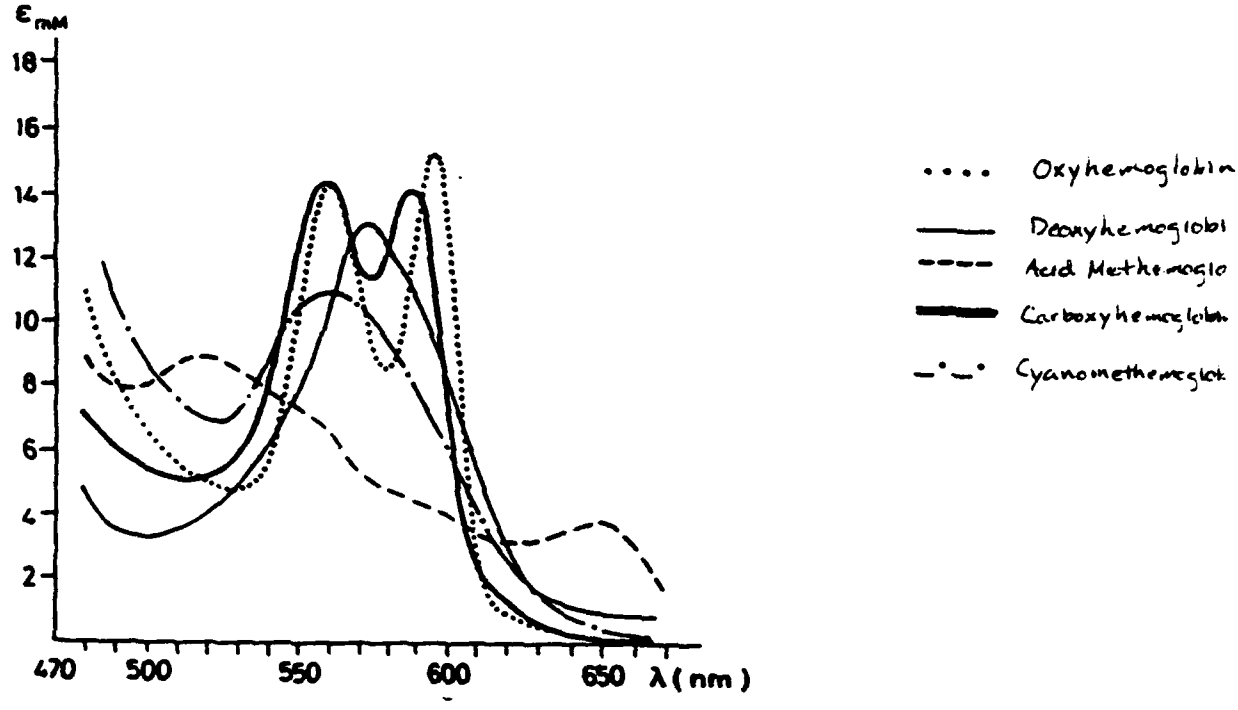

Figure 1a: Visible Spectra of Hemoglobin Derivatives

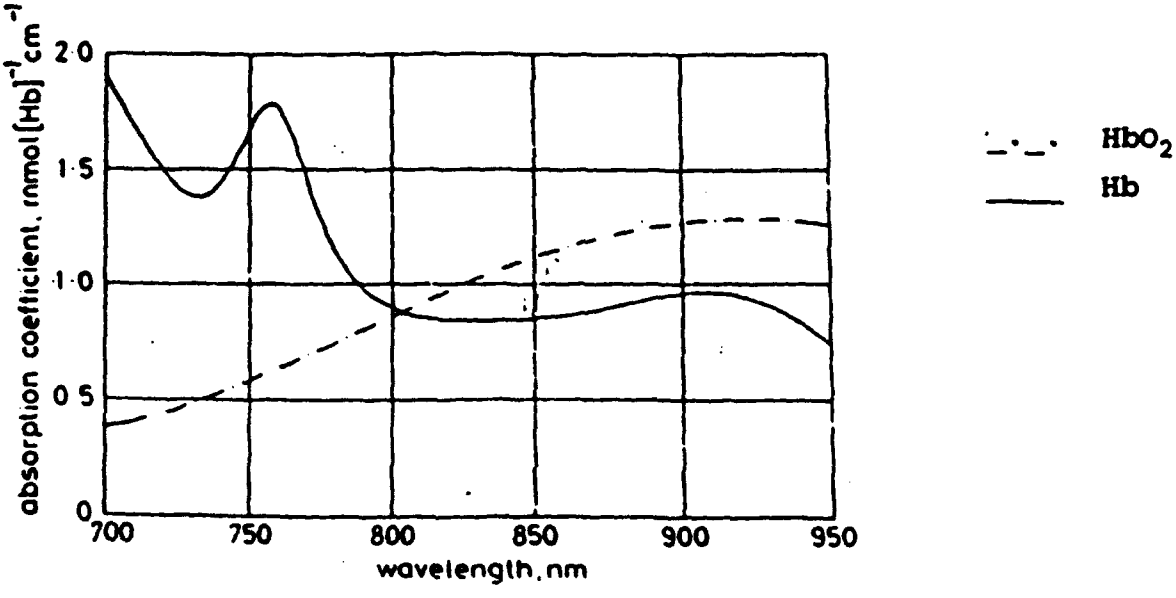

Figure 1b: Short-wave Near-infrared Spectra of Hemoglobin

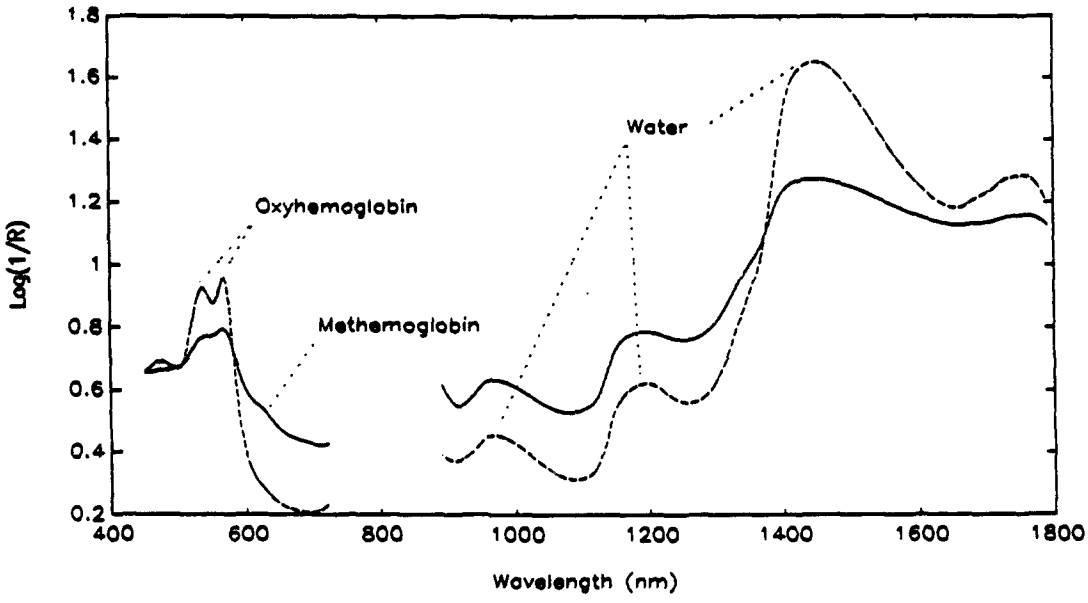

Figure 2. Typical spectra of burn wounds. (--) shallow and (—) deep injuries.

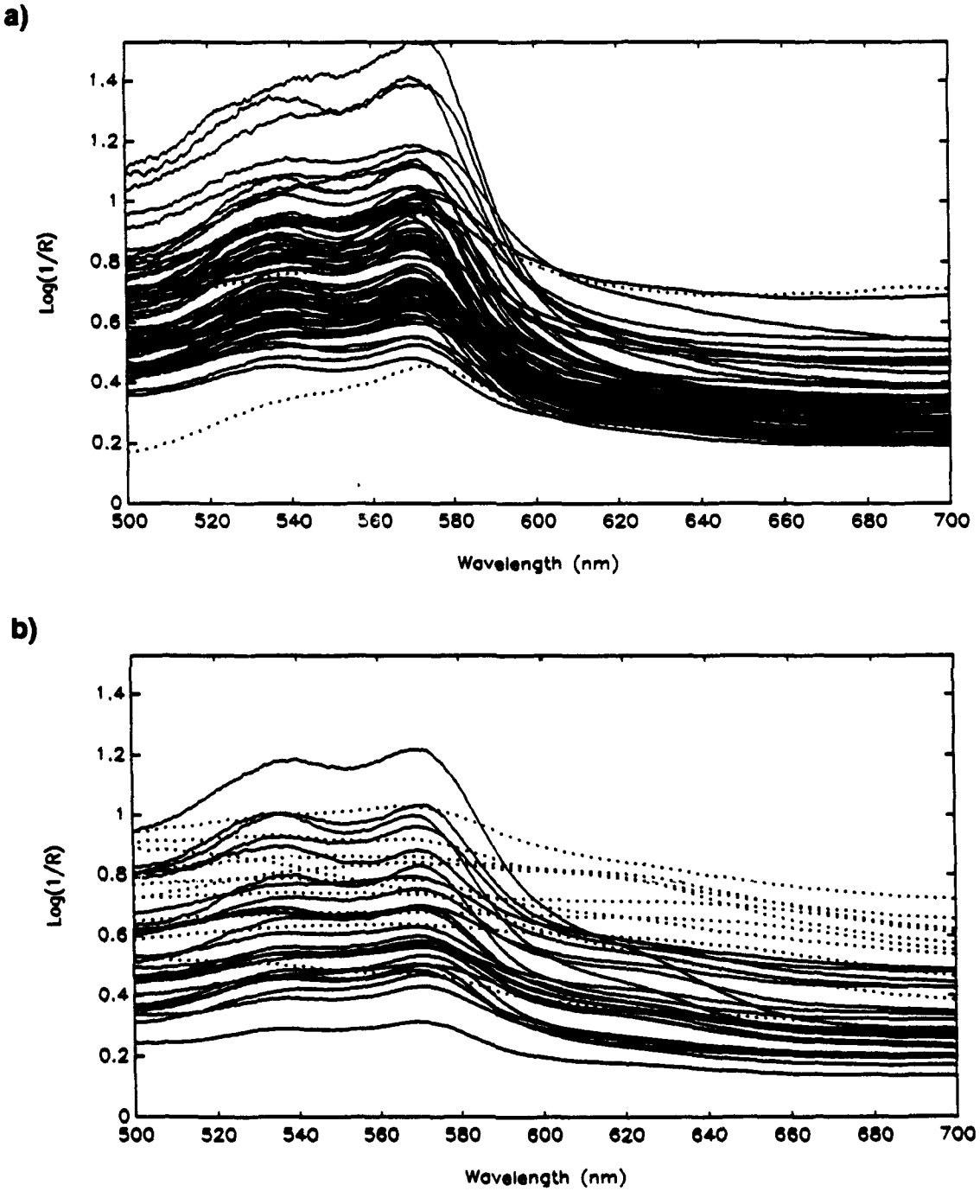

Figure 3. Aggregate spectra of burn wounds. a) shallow and b) deep injuries.

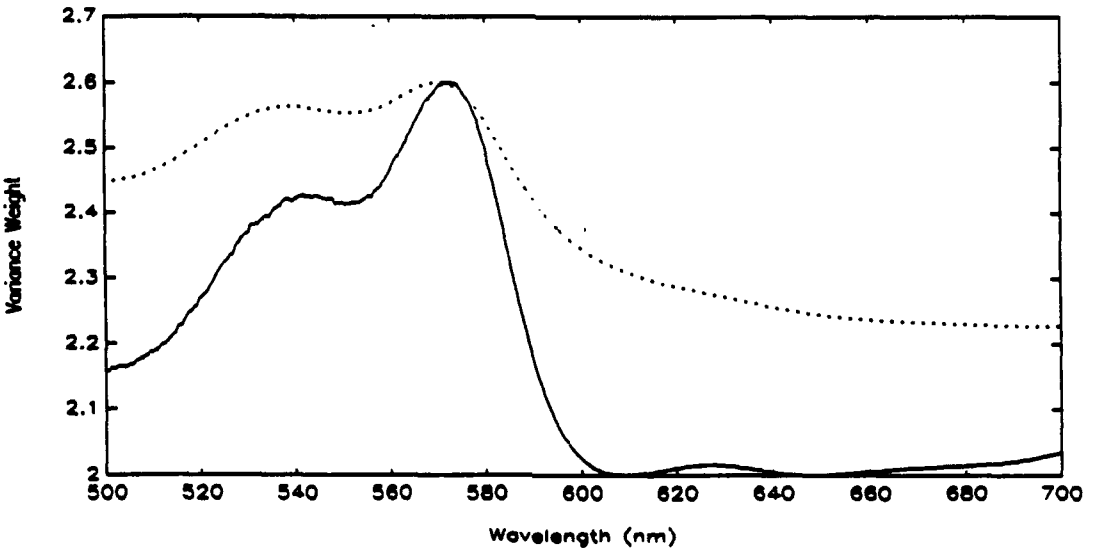

Figure 4. Variance weigths of raw spectra. (—) variance weights (• •) mean spectrum.

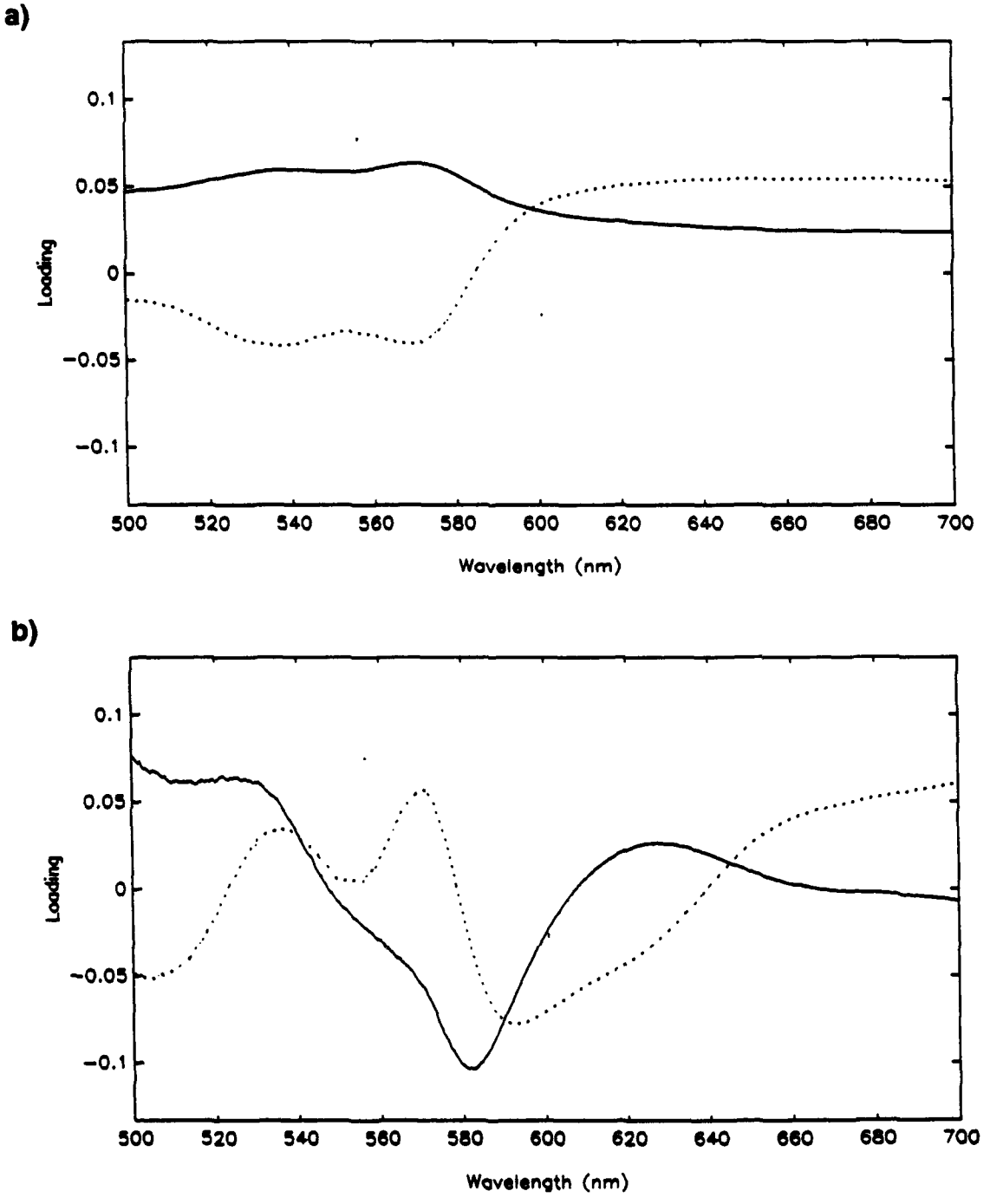

Figure 5. Loadings from principal component analysis of raw spectra. Eigenvectors c) 1 and 2, d) 3 and 4. Eigenvectors (-) 1 and 3 (...) 2 and 4.

c)

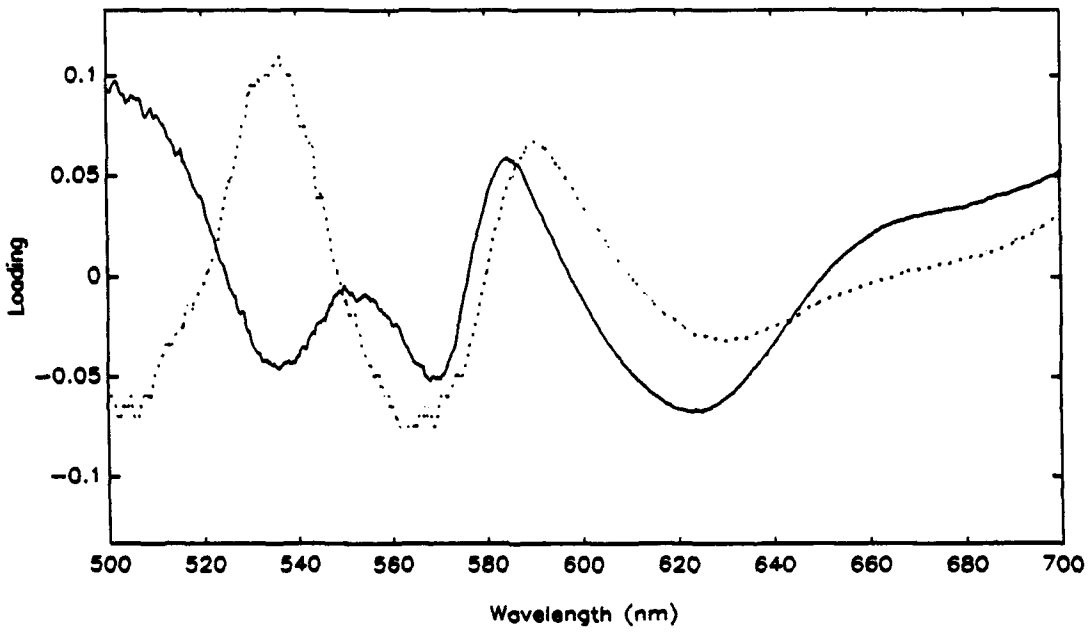

d)

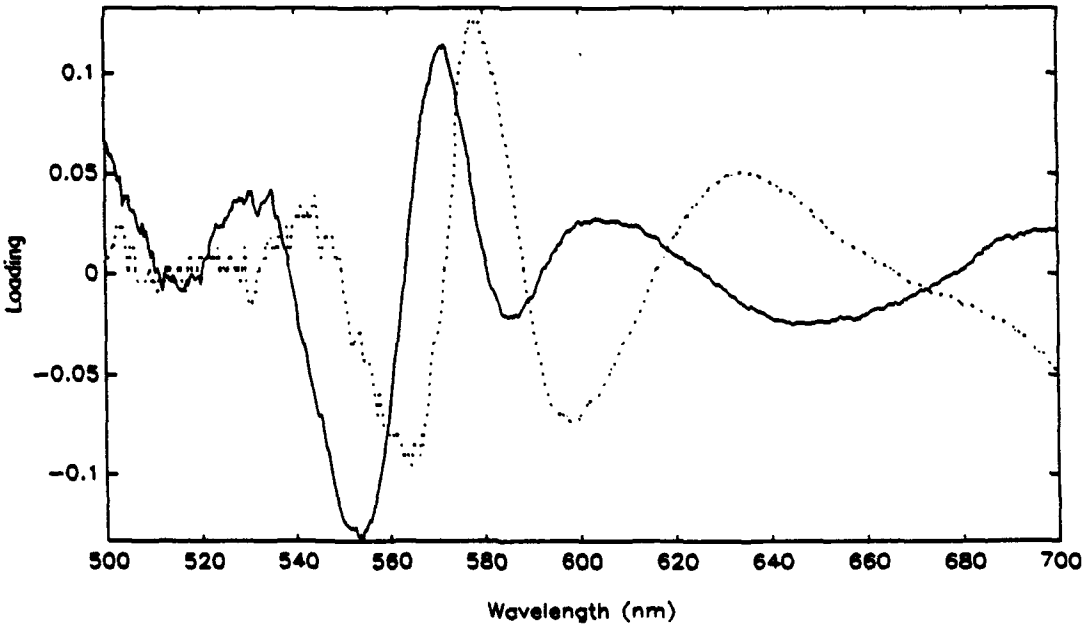

Figure 5. Loadings from principal component analysis of raw spectra. Eigenvectors a) 5 and 6, b) 7 and 8. Eigenvectors (-) 5 and 7 (...) 6 and 8.

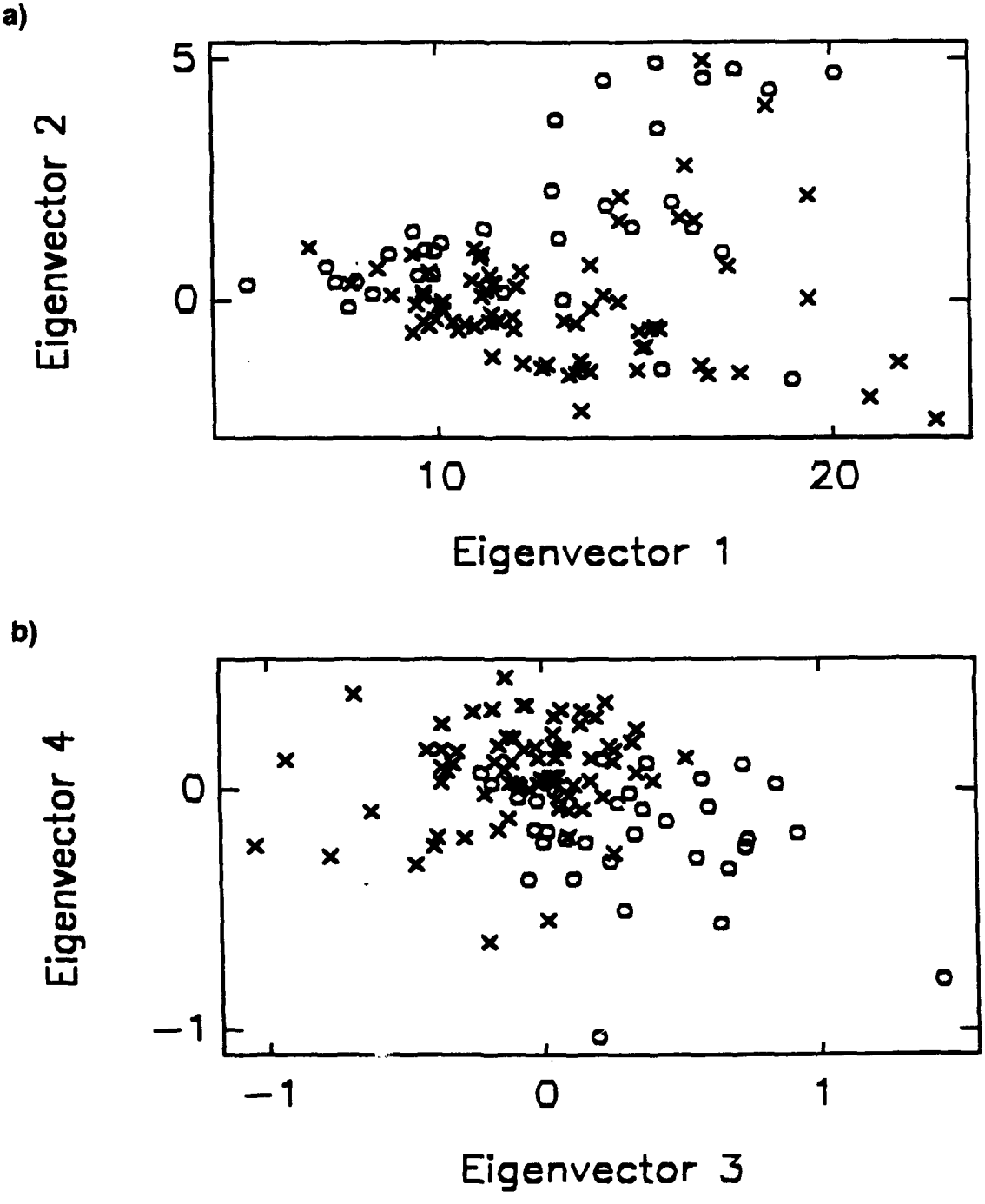

Figure 6. Scores from principal component analysis of raw spectra. (x) shallow and (o) deep injuries.

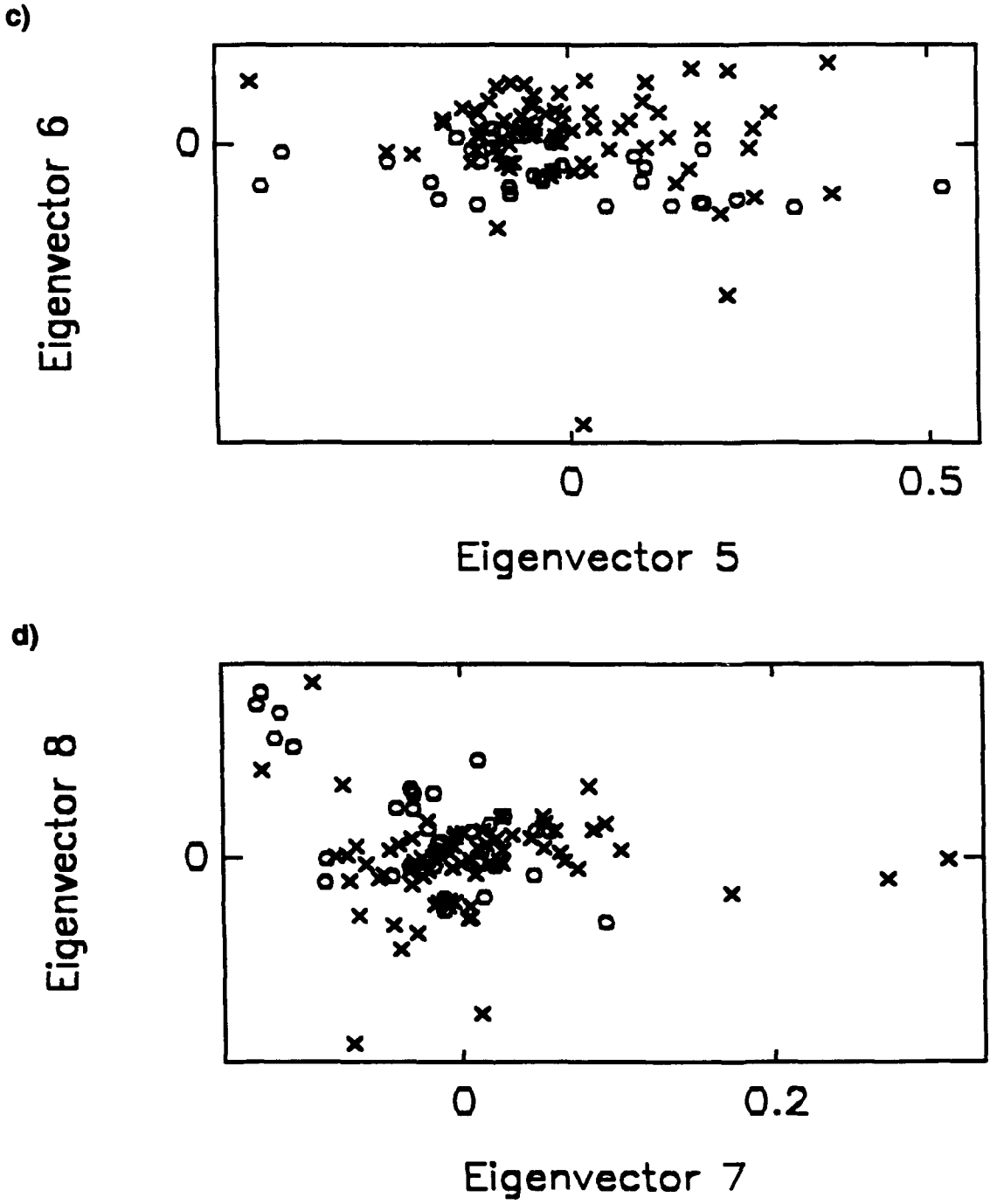

Figure 6. Scores from principal component analysis of raw spectra. (x) shallow and (o) deep injuries.

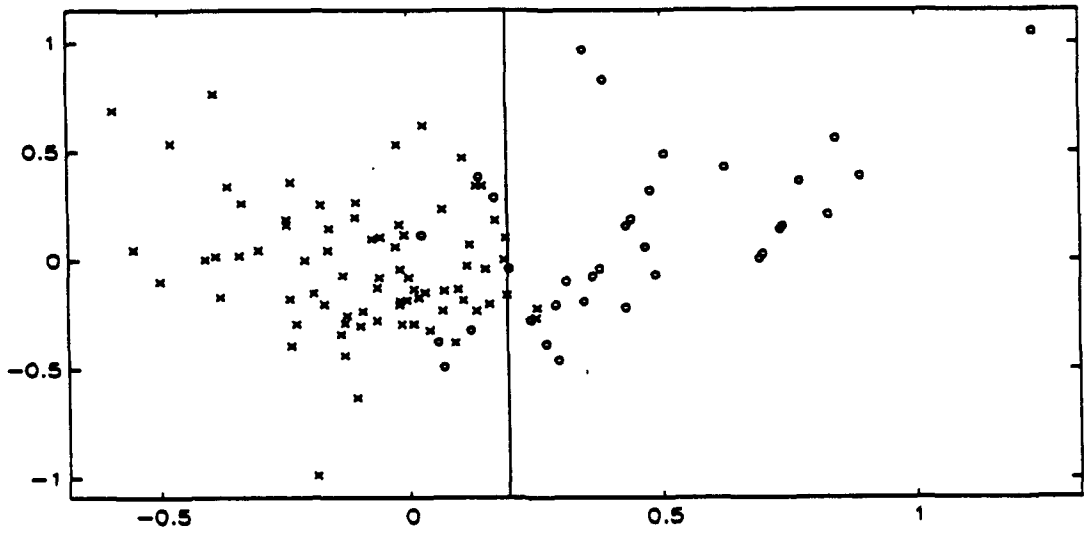

Figure 7. Rotated PCA scores from raw spectra. (x) shallow and (o) deep injuries.

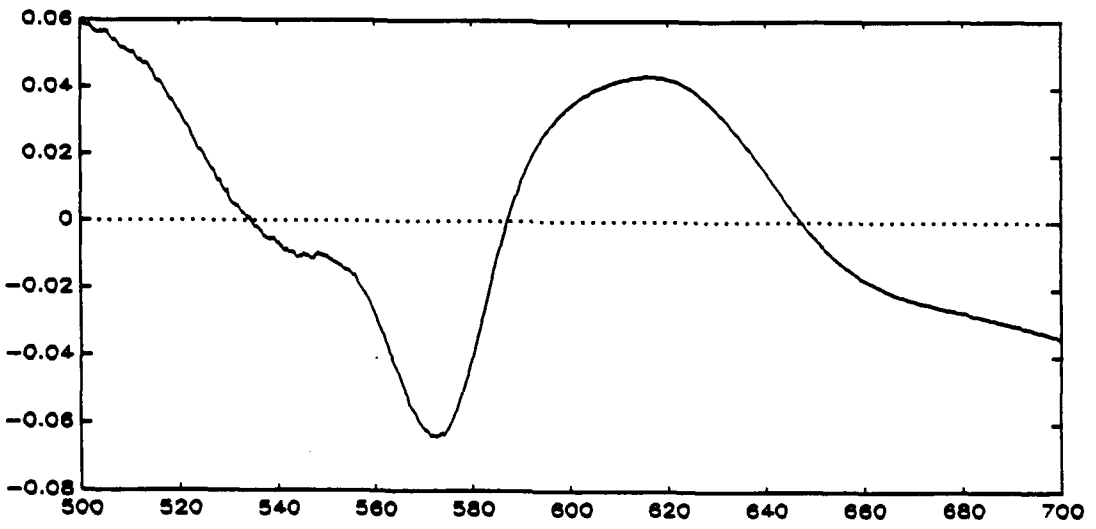

Figure 8. First rotated PCA loading from raw spectra.

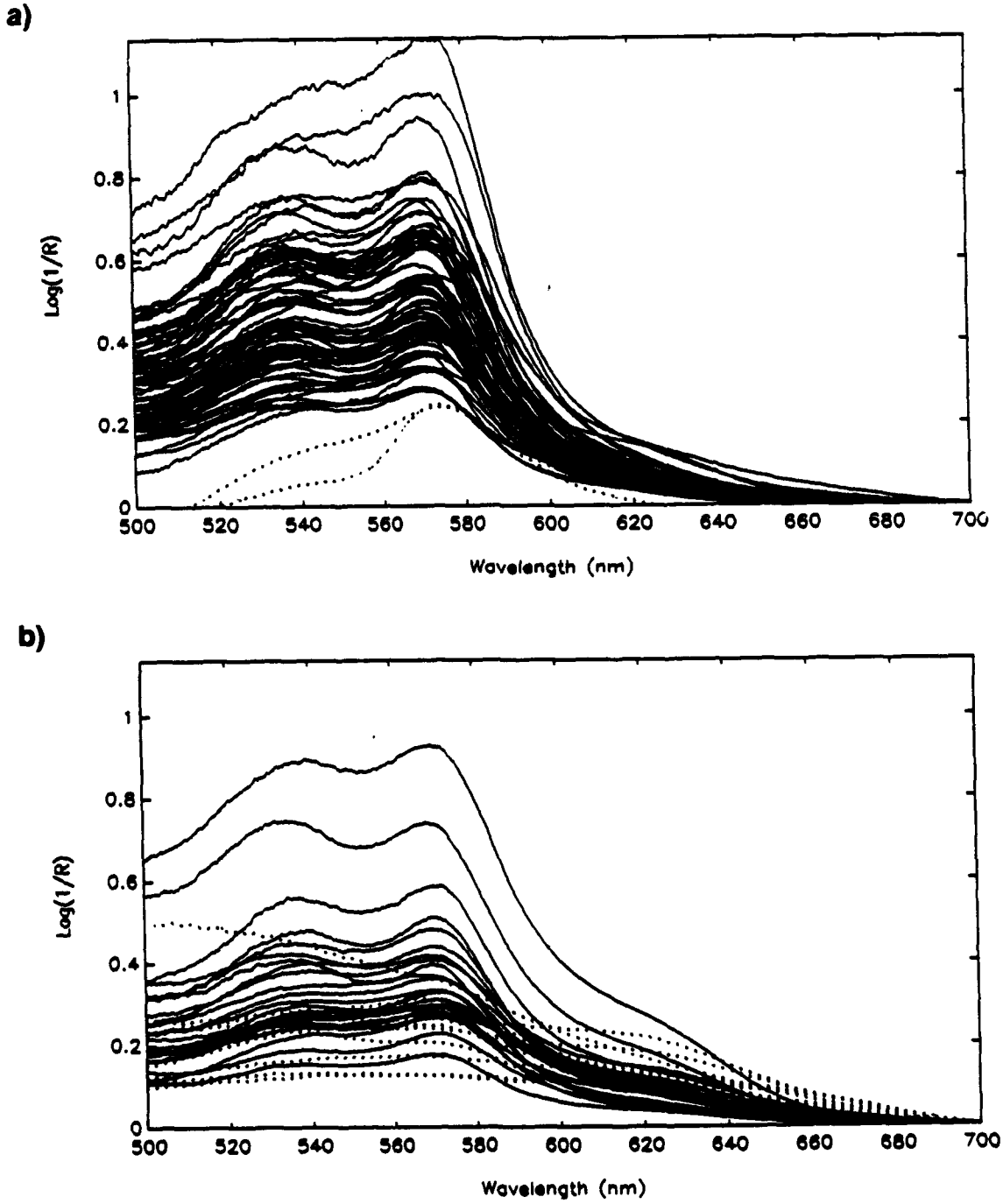

Figure 9. Baseline-subtracted spectra. a) shallow and b) deep injuries.

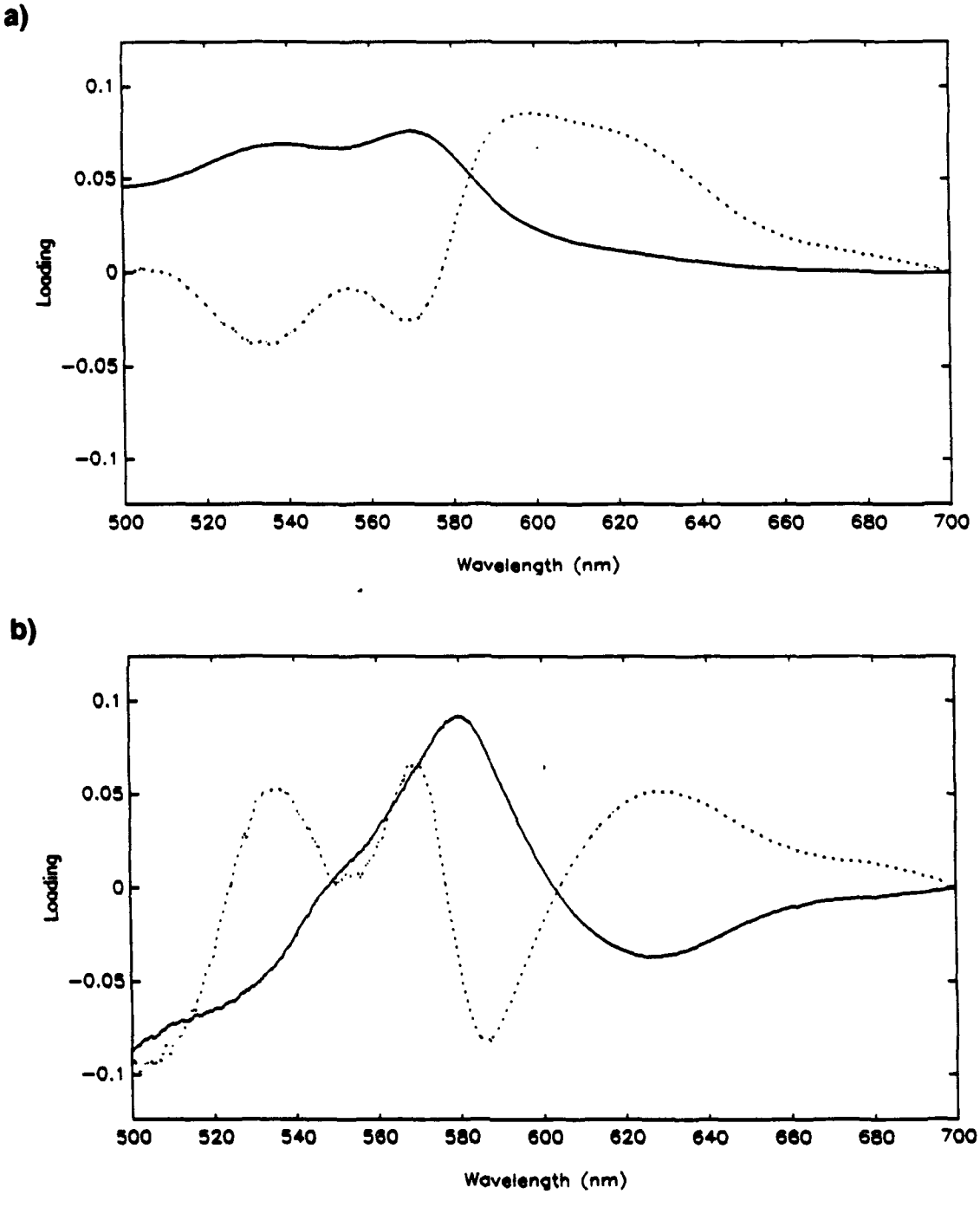

Figure 10. Loadings from principal component analysis of baseline-subtracted spectra. Eigenvectors a) 1 and 2, b) 3 and 4. Eigenvectors (-) 1 and 3 and (...) 2 and 4.

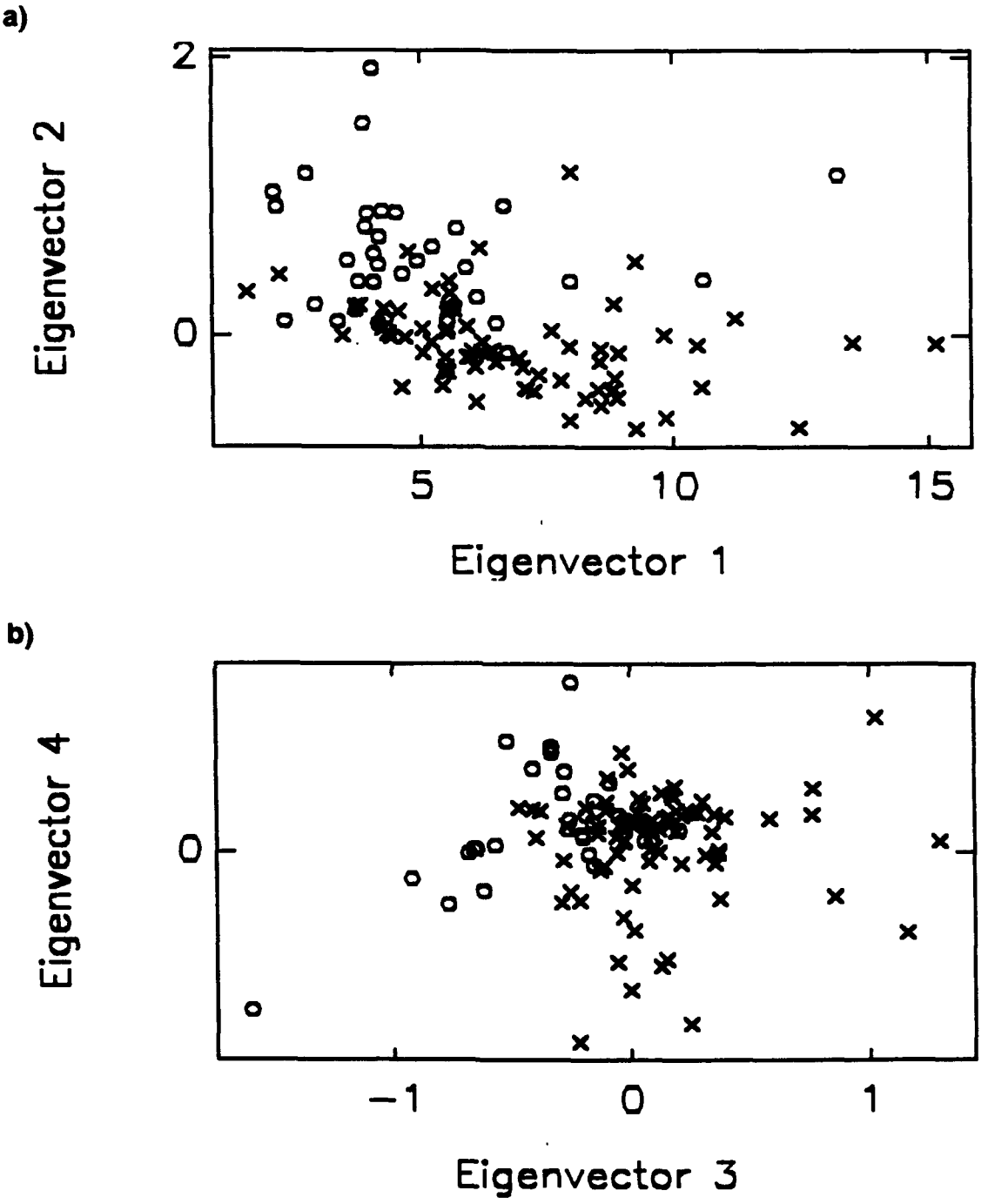

Figure 11. Scores from principal component analysis of baseline-subtracted spectra. (x) shallow and (o) deep injuries.

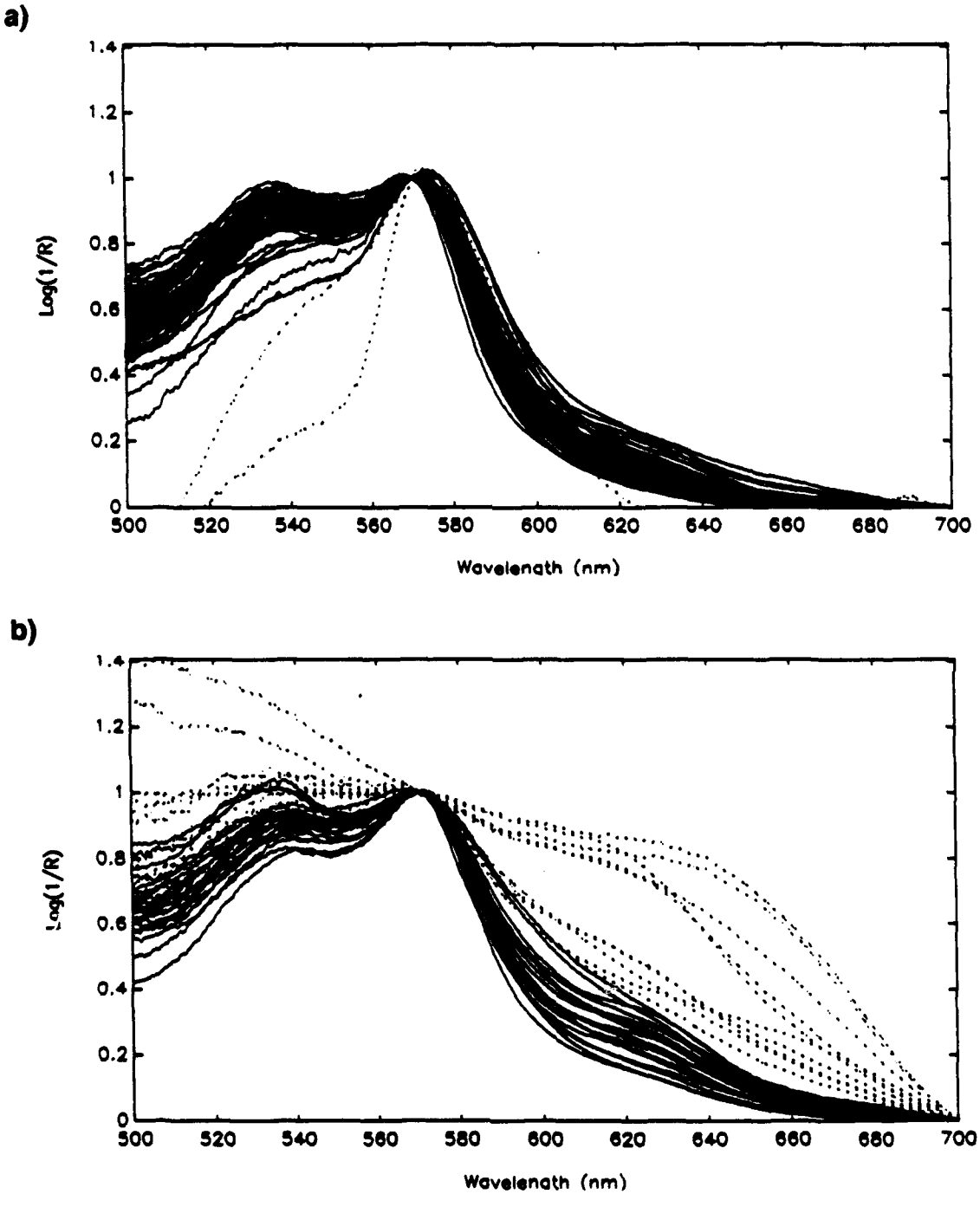

Figure 12. Normalized spectra of burn wounds. a) shallow and b) deep injuries.

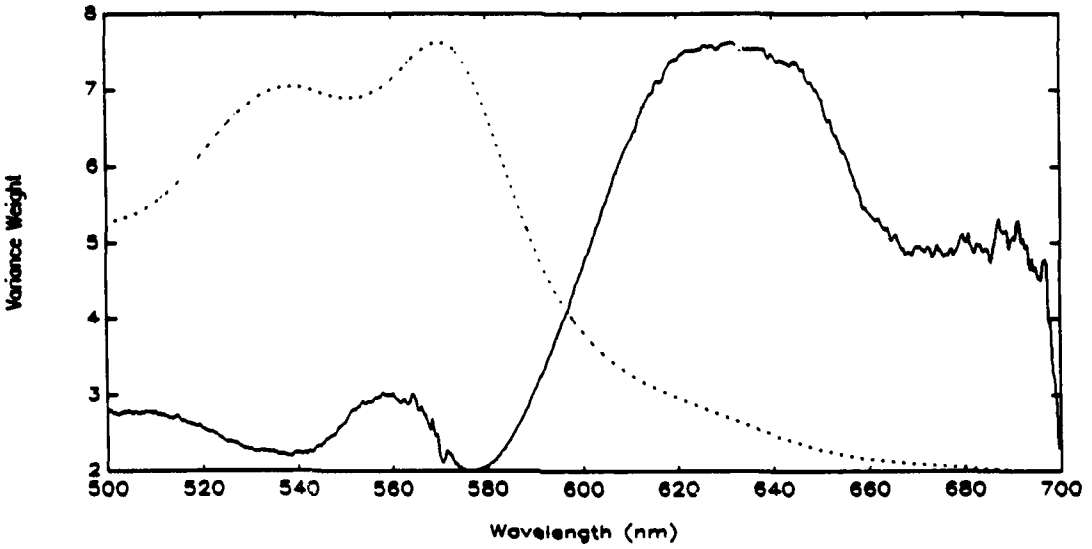

Figure 13. Variance weigths of single-wavelength normalized spectra. (—) variance weights (• •) mean spectrum.

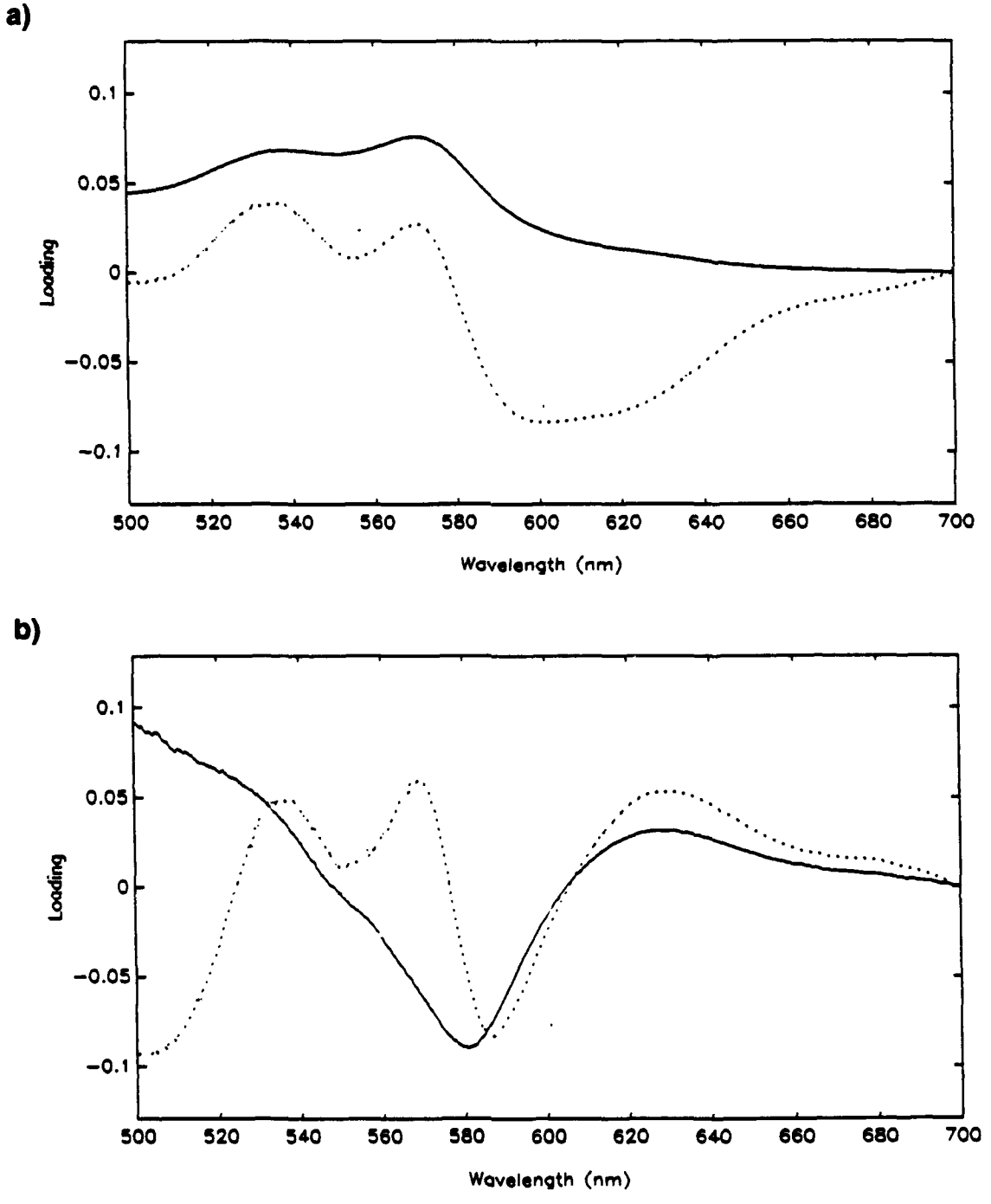

Figure 14. Loadings from principal component analysis of normalized spectra. Eigenvectors a) 1 and 2, b) 3 and 4. Eigenvectors (-) 1 and 3, (...) 2 and 4.

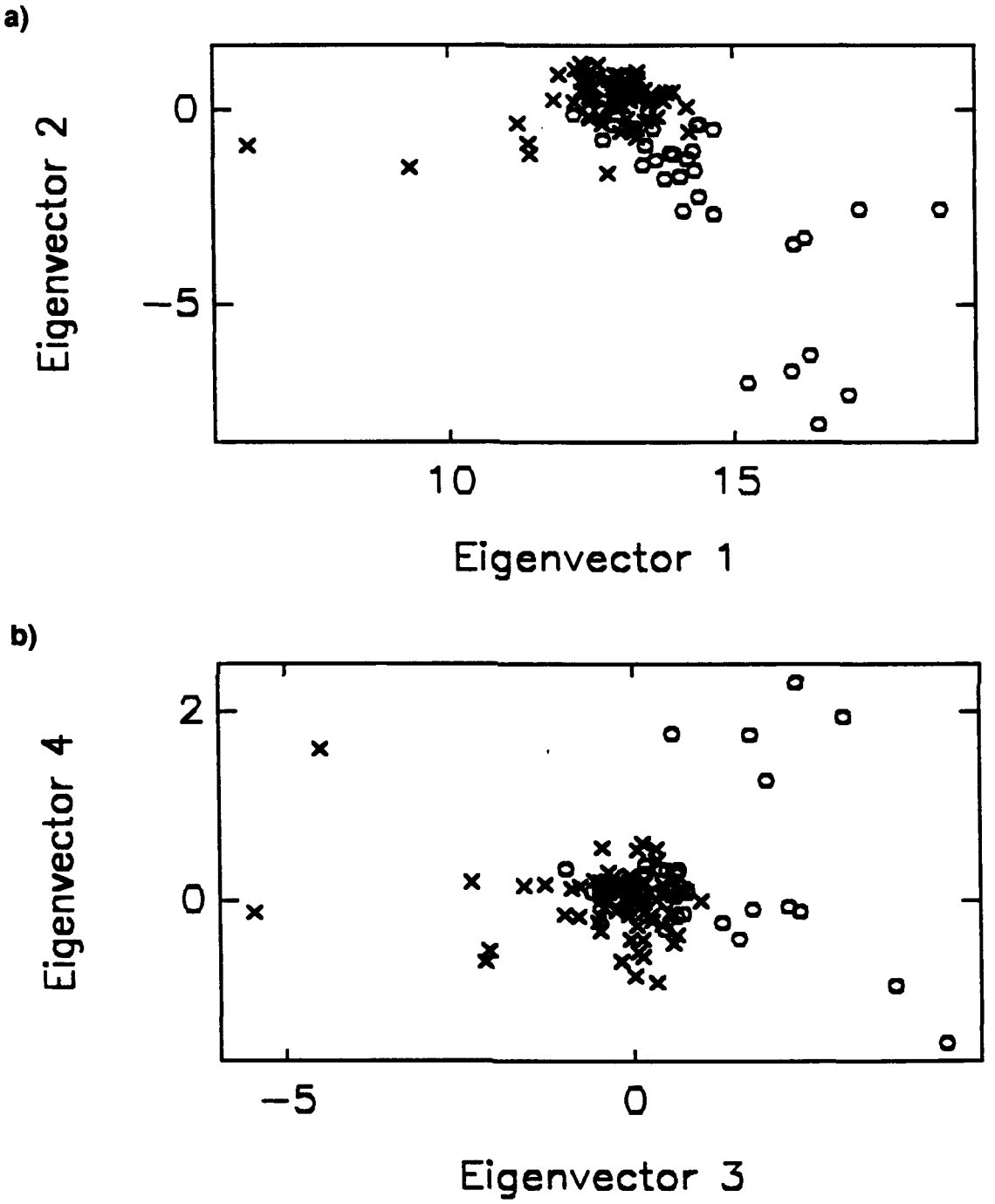

Figure 15. Scores from principal component analysis of normalized spectra. (x) shallow and (o) deep injuries.

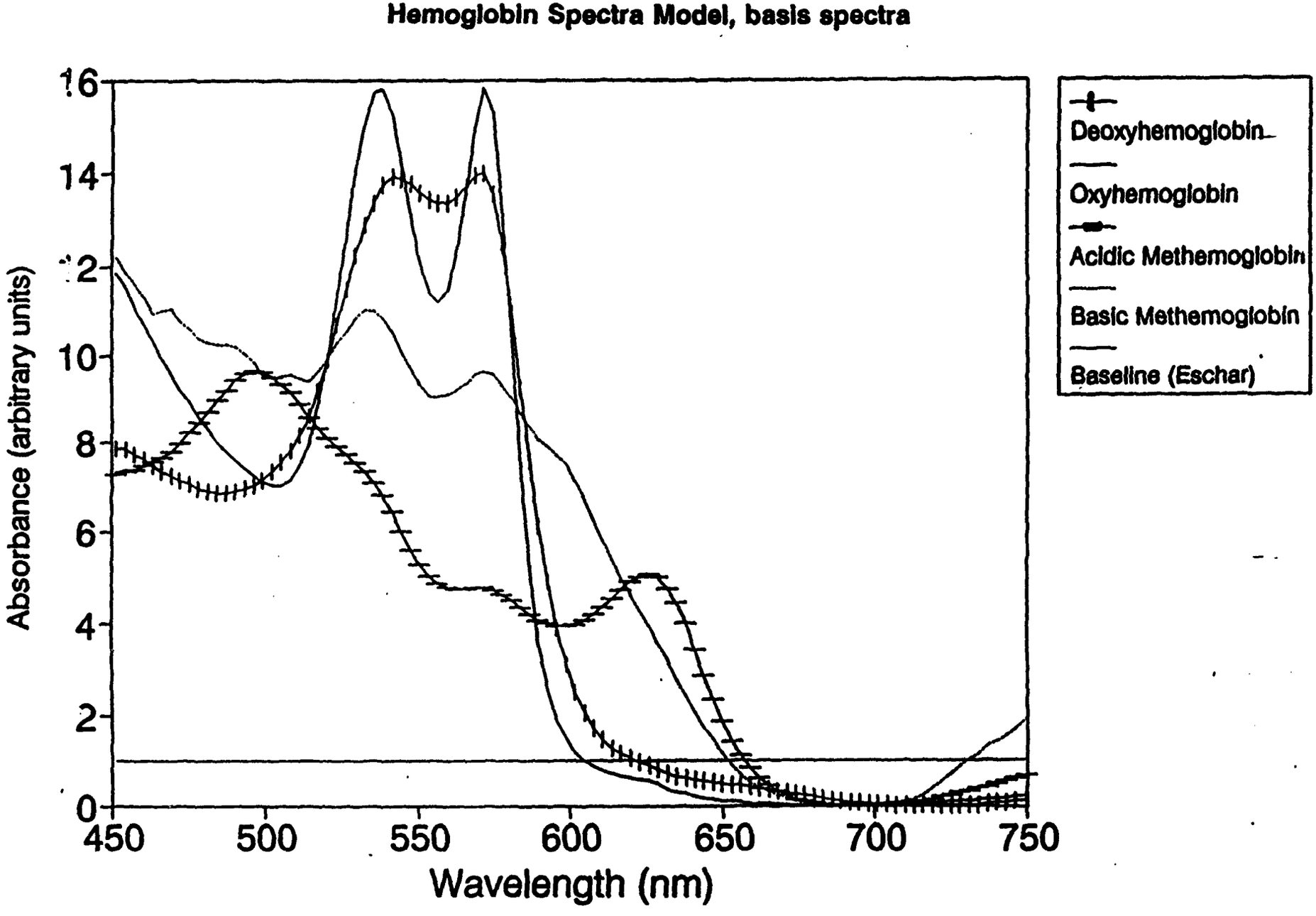
Hemoglobin Spectra Model, basis spectra
Absorbance (arbitrary units)
0
2
4
6
8
10
12
14
16
450
500
550
600
650
700
750
Wavelength (nm)
Deoxyhemoglobin
Oxyhemoglobin
Acidic Methemoglobin
Basic Methemoglobin
Baseline (Eschar)

Figure 16

Hemoglobin Spectra Model, fitted spectra

Shallow

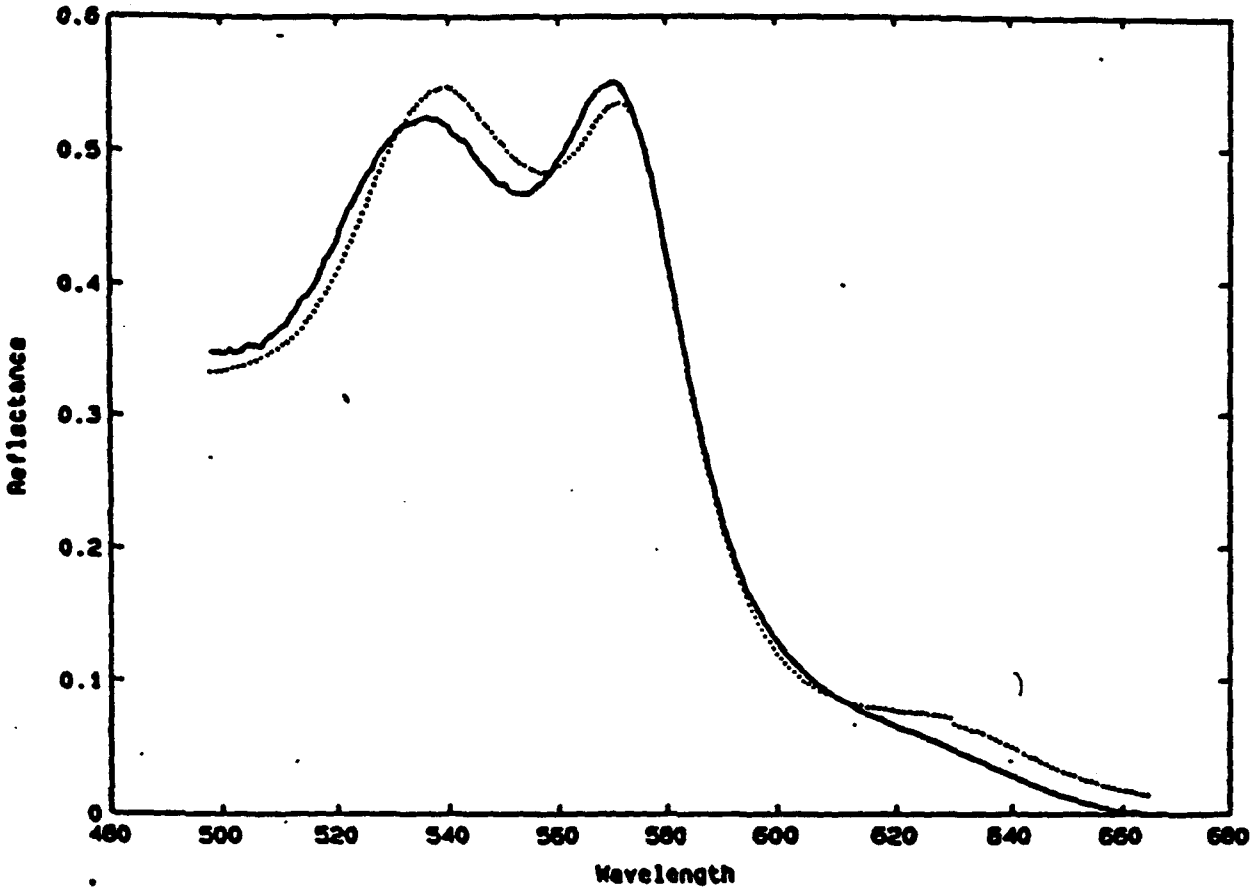

Deep

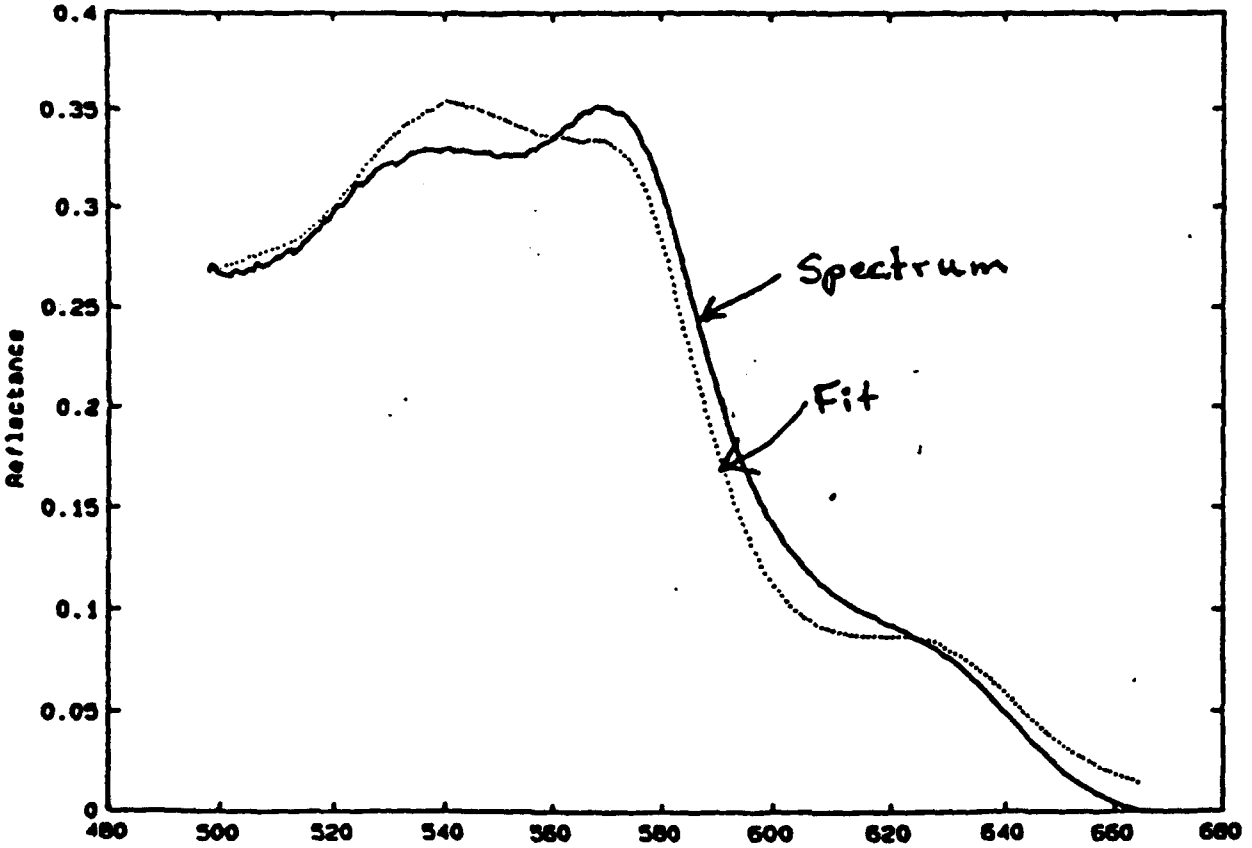

Figure 17

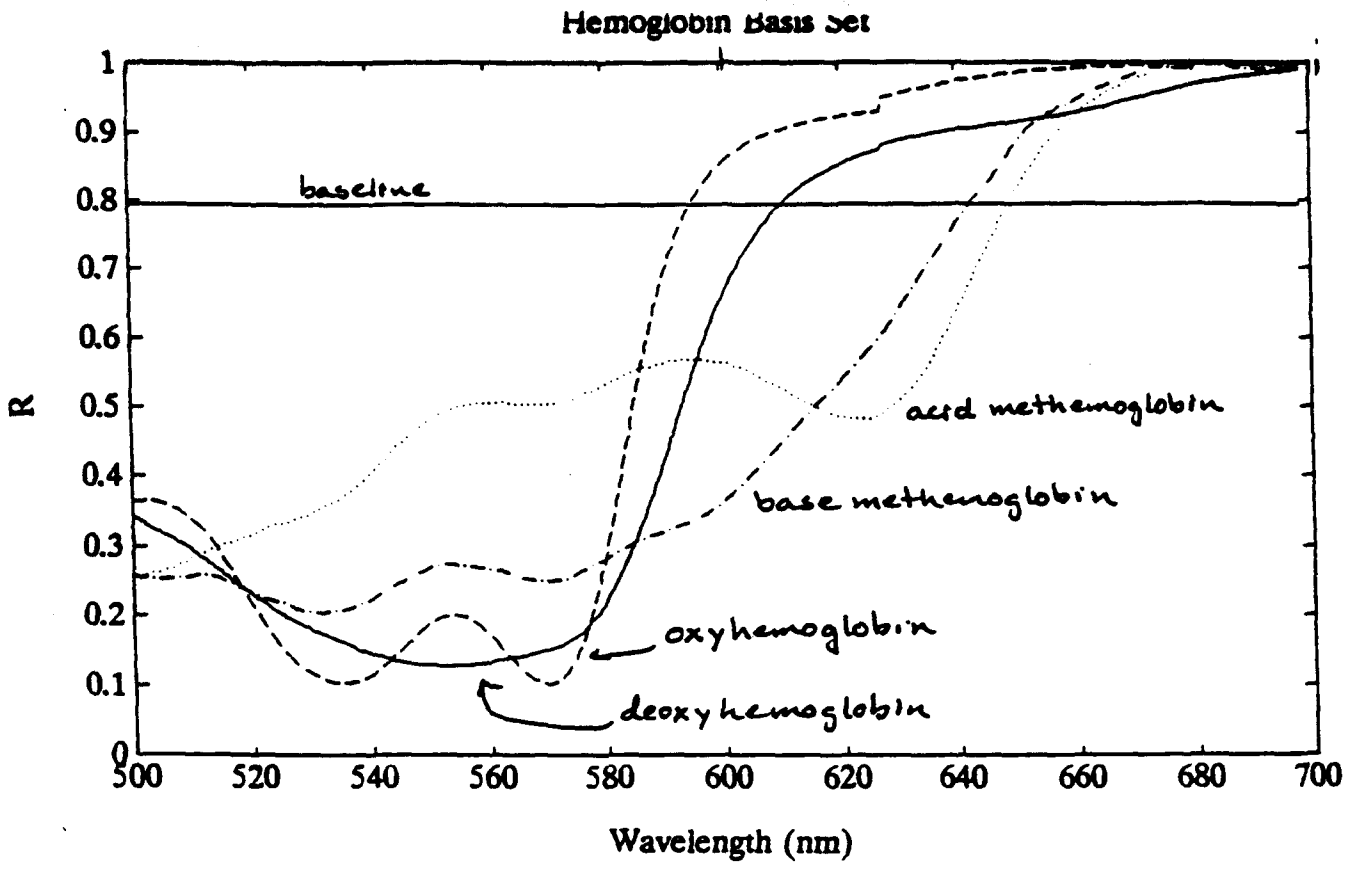
Hemoglobin Basis Set
baseline
acid methemoglobin
base methemoglobin
oxyhemoglobin
deoxyhemoglobin
R
Wavelength (nm)

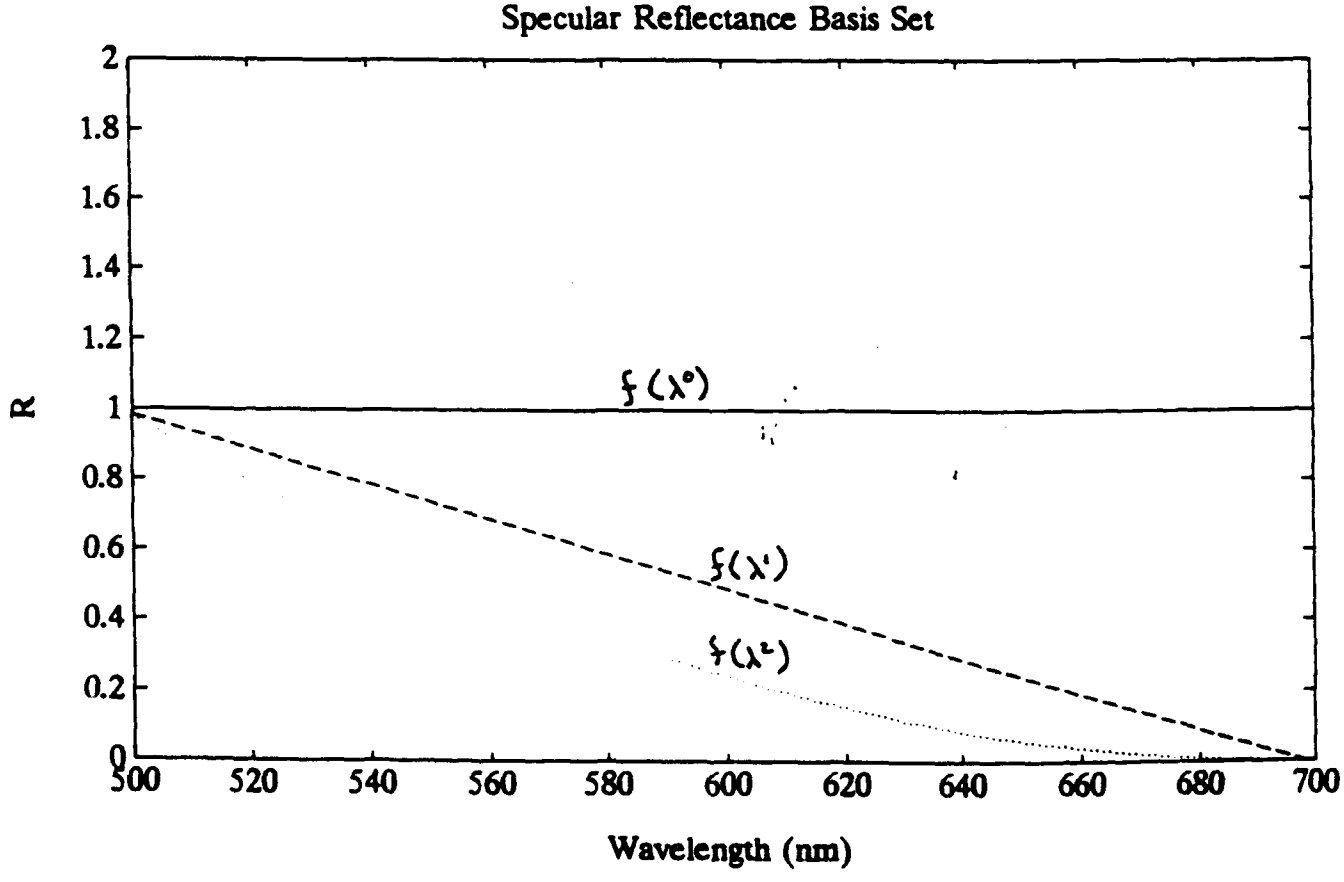
Specular Reflectance Basis Set
f(λ°)
f(λ¹)
f(λ²)
R
Wavelength (nm)

Figure 18

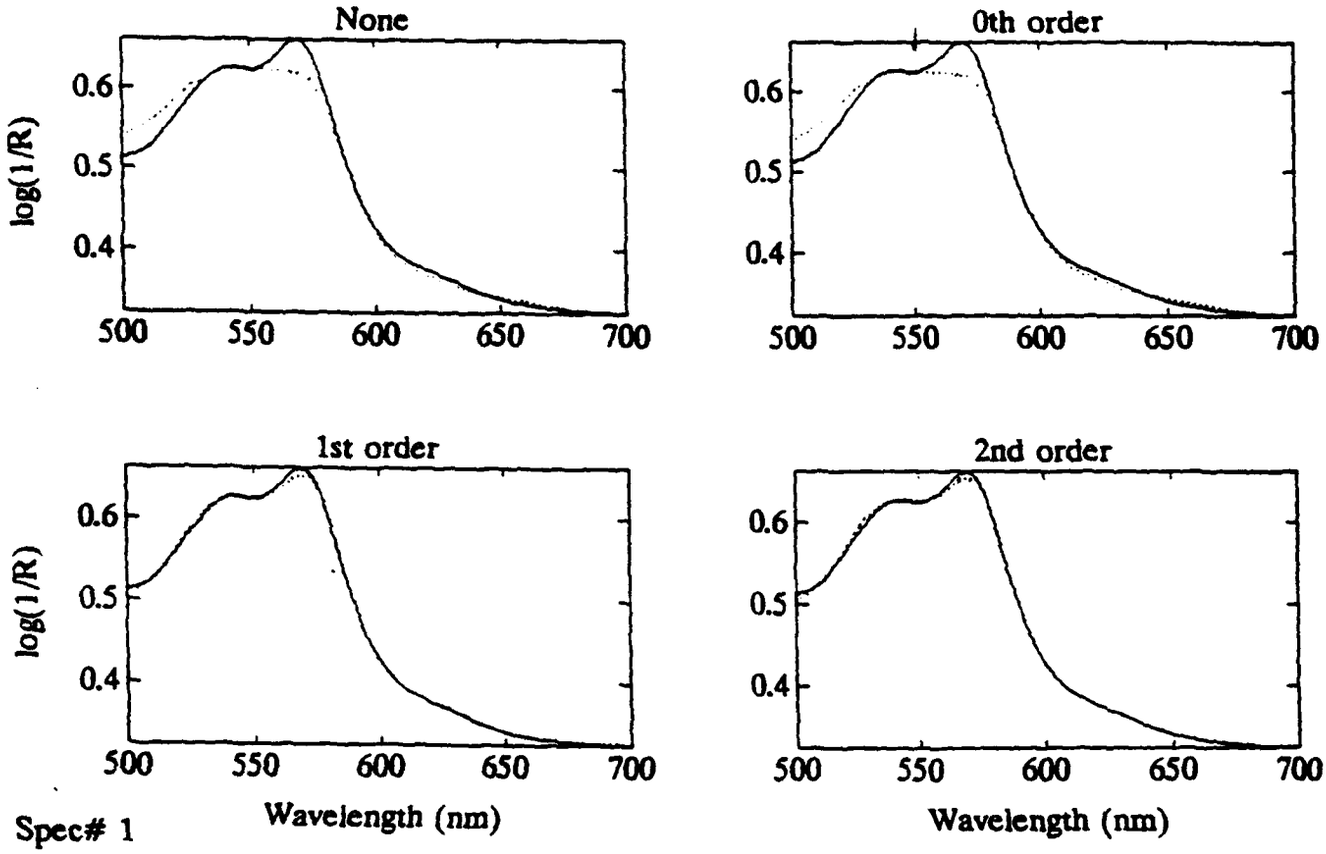

Figure 18 Spectrum of a shallow burn (—) spectrum, (...) fitted spectrum

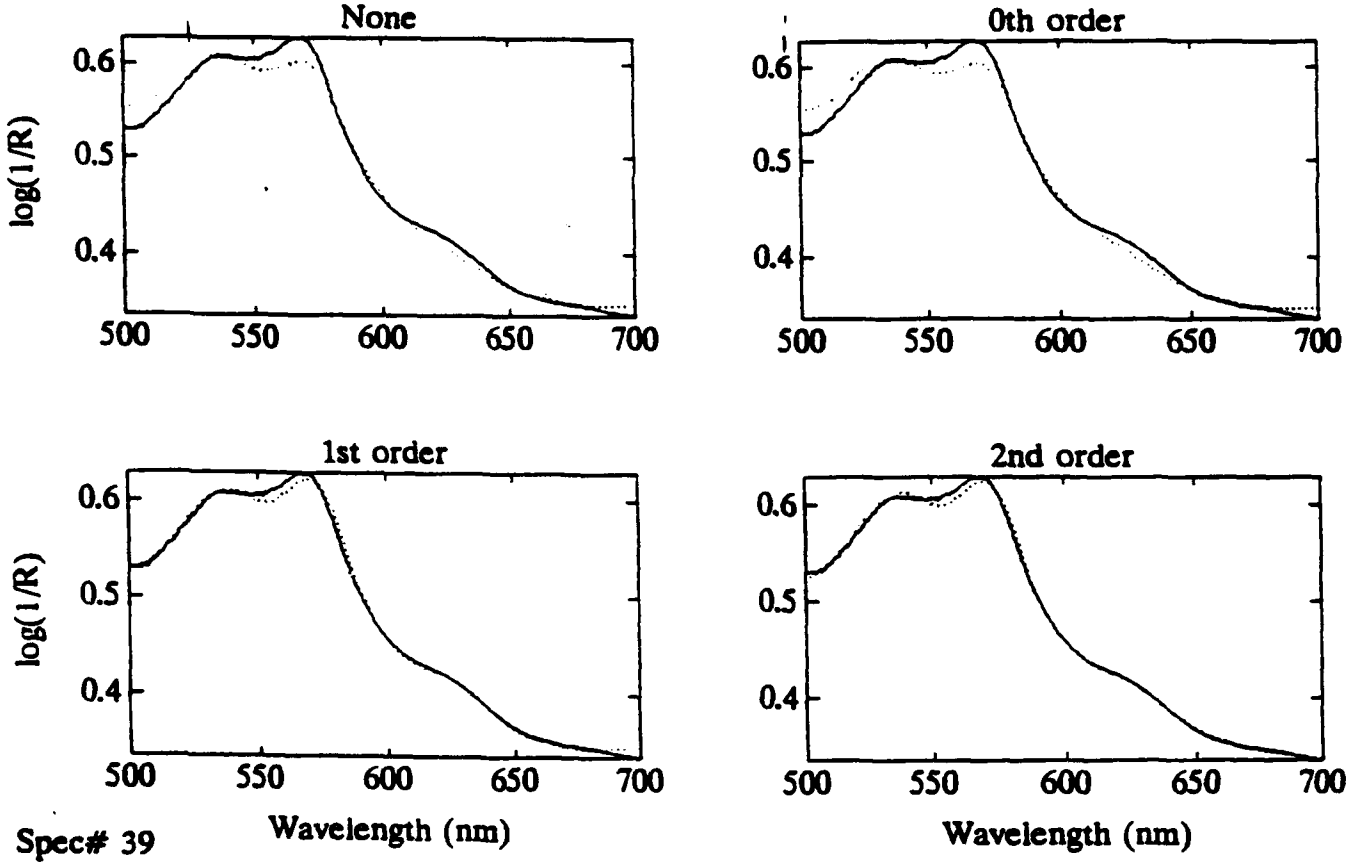

Figure 19 Two-layer, hemoglobin spectra model. (—) spectrum of a deep burn (···) reconstructed spectrum

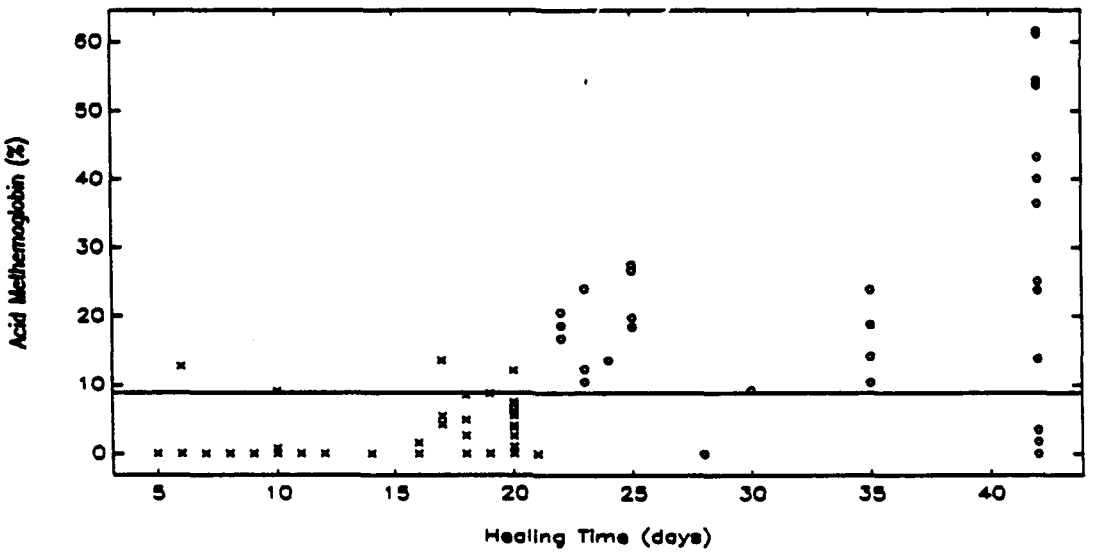

Figure 21. Relative acid methemoglobin concentration. (x) shallow and (o) deep *injuries.*

A

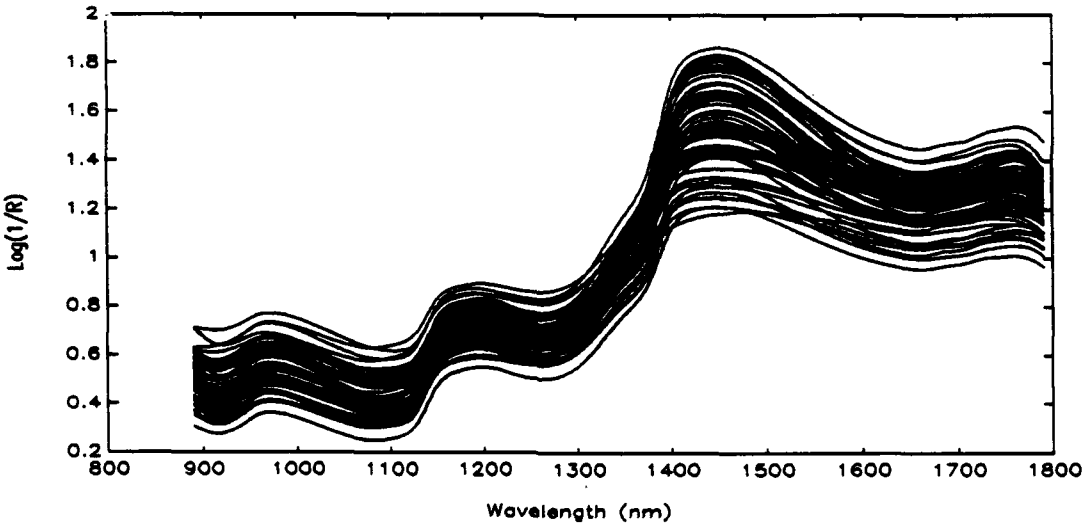

B

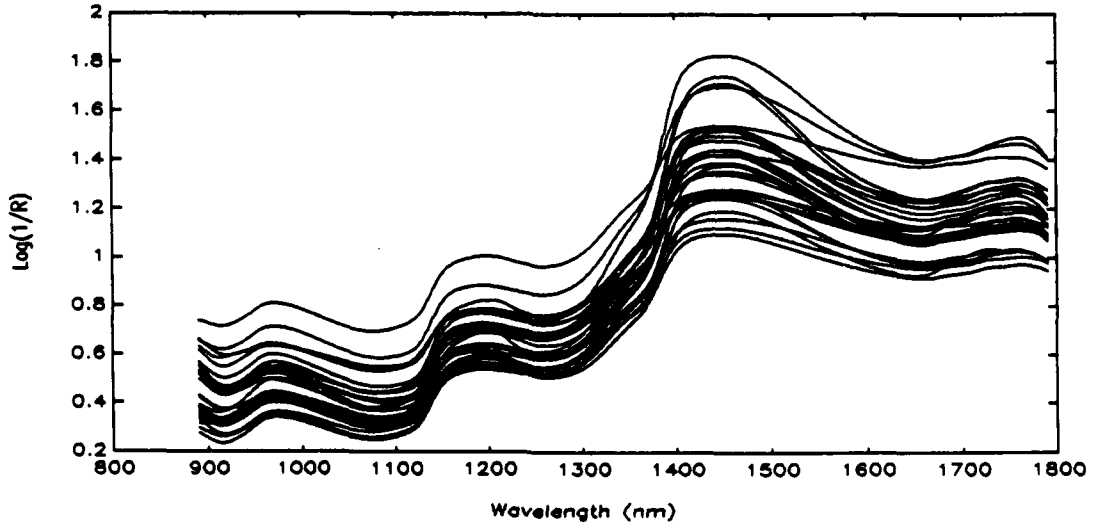

Figure 22.
Near infrared spectra of burn wounds. (a) shallow and (b) deep burns.

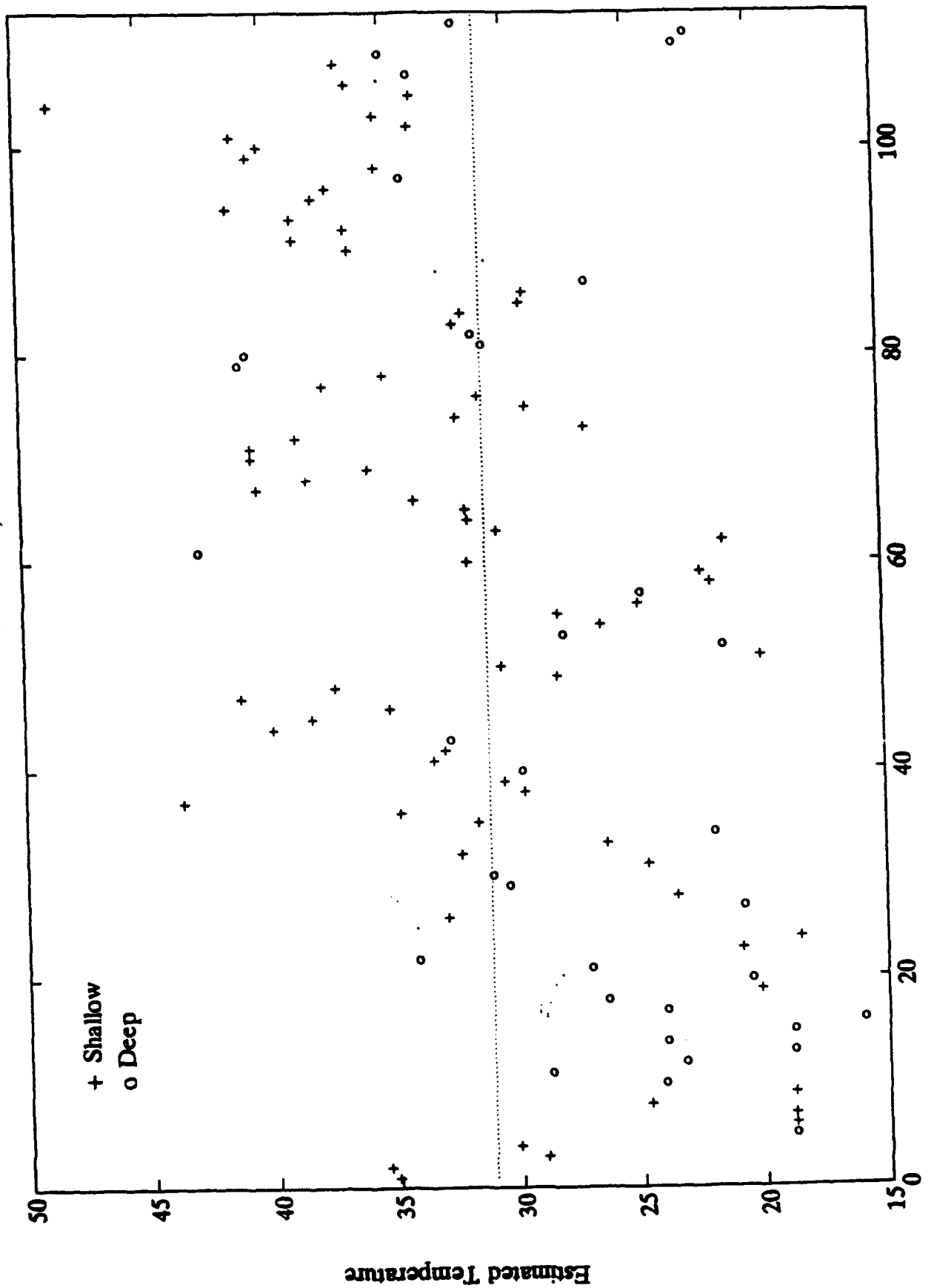
Skin Temperature Model
+ Shallow
o Deep
Estimated Temperature
Sample number
50
45
40
35
30
25
20
15
0
20
40
60
80
100

Figure 2.3

A

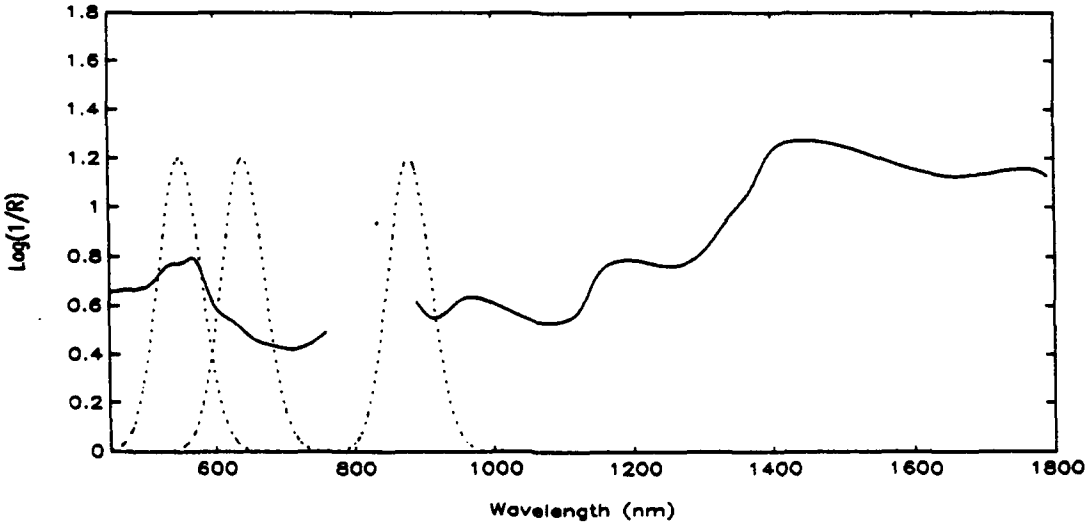

Figure 24.a Burn Depth Indicator Simulation. (—) a typical spectrum of a deep burn, and (• • •) the LED output functions.

B

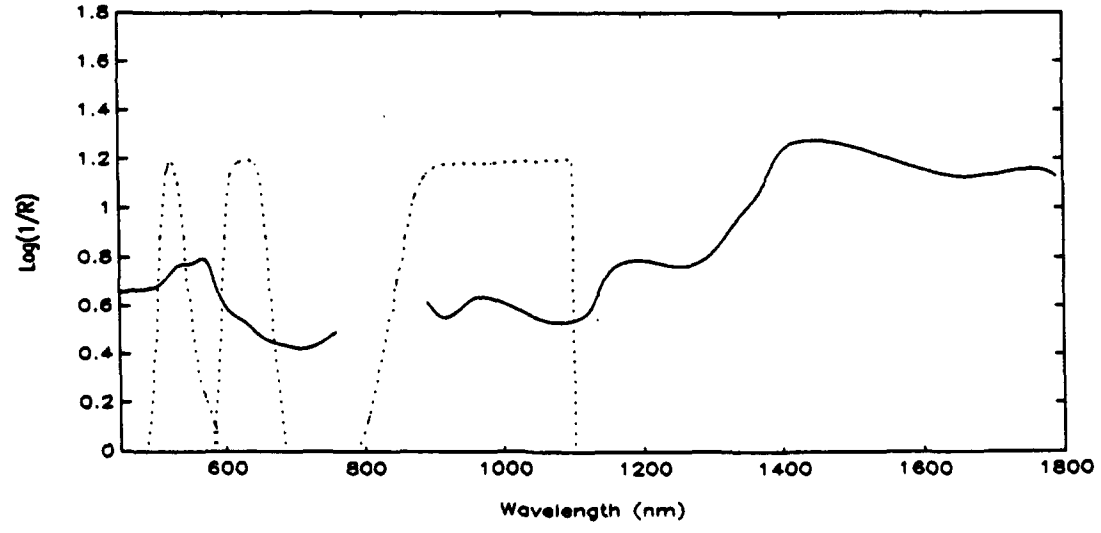

Figure 24.b Imaging Burn Depth Indicator Simulation. (—) a typical spectrum of a deep burn, and (• • •) the filter transmittance functions.

a)

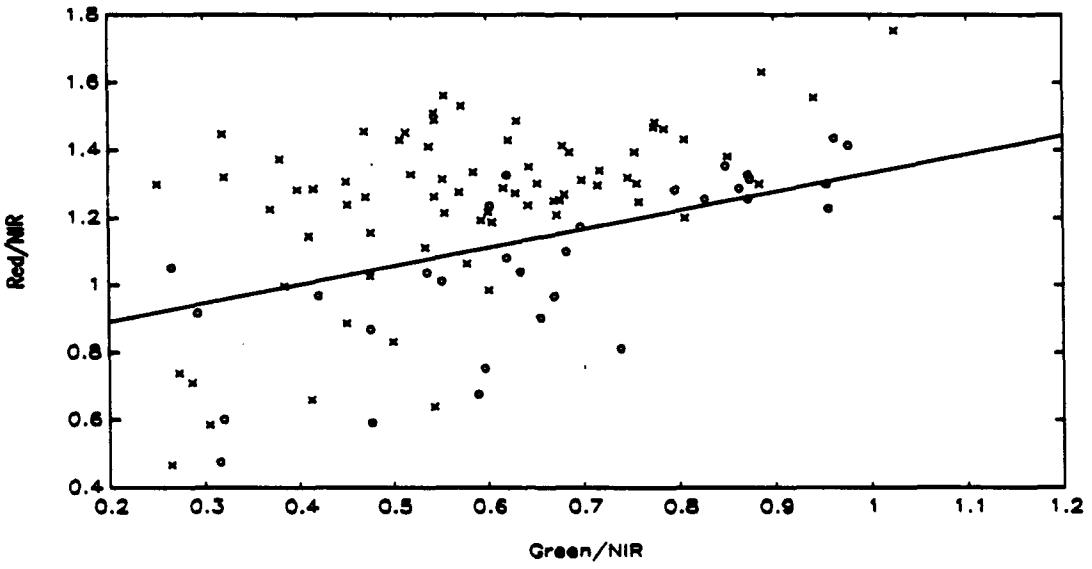

b)

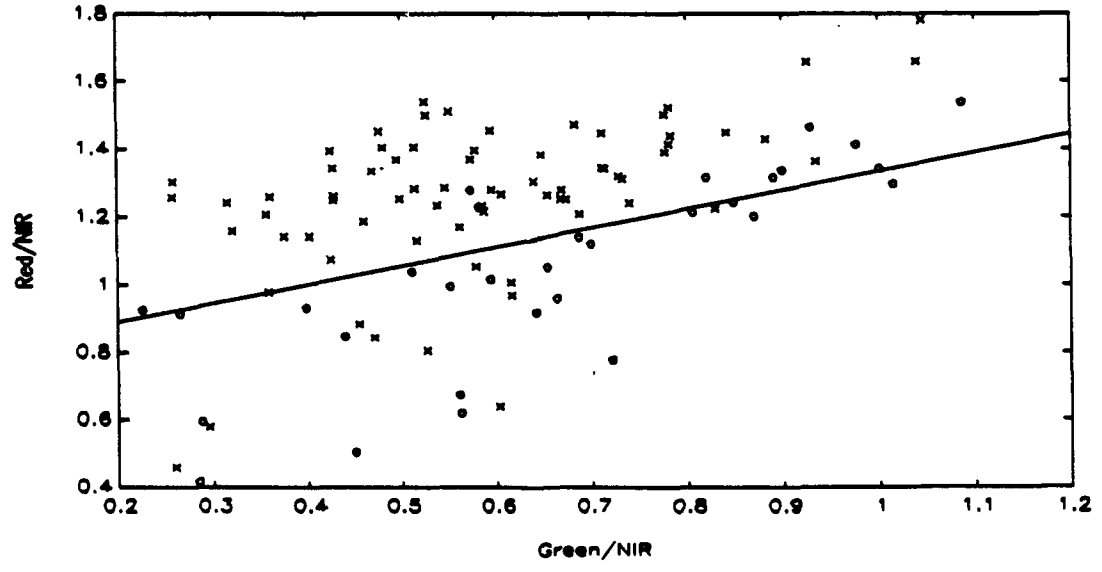

Figure 25. Simulated instrument responses. (a) the burn depth indicator, (b) the imaging burn depth indicator. (x) are responses for shallow burns, (o) for deep burns. (-) is the best discriminant line found by vanLiew.

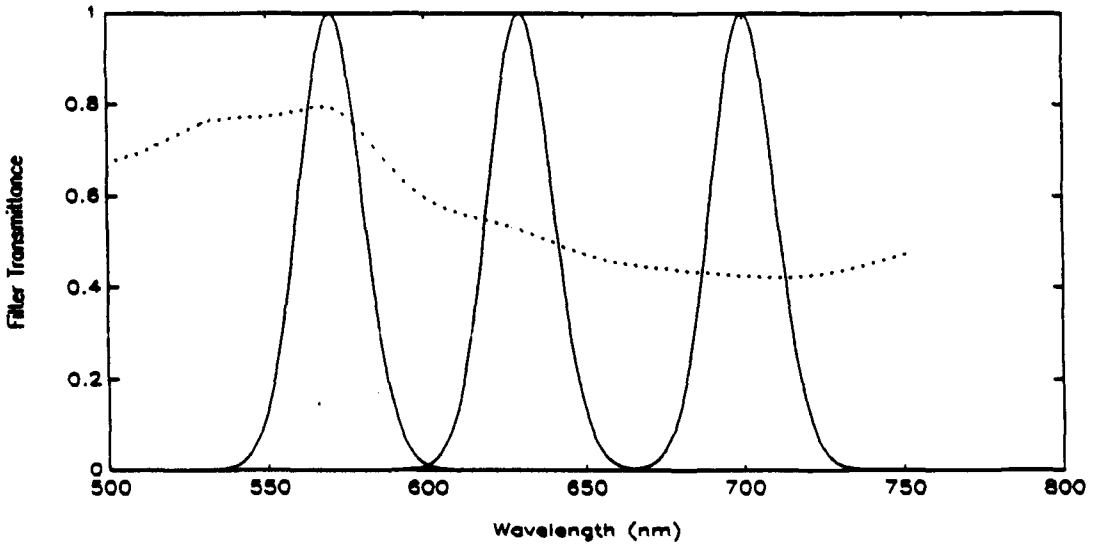

Figure 26. Filters chosen for the proposed IBDI model. (—) filters and (• •) spectrum of a deep burn.

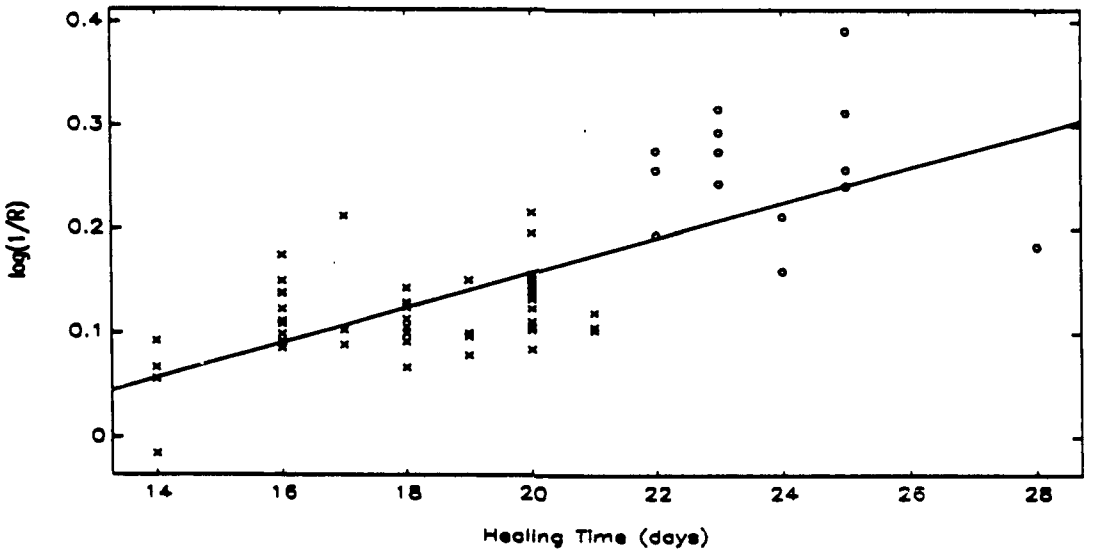

Figure 27. Simulated response of the proposed IBDI algorithm. (x) shallow and (o) deep injuries.